Aqueous organic redox flow batteries

Vikram Singh[1,2,§], Soeun Kim[1,2,§], Jungtaek Kang[1], and Hye Ryung Byon[1,2] (✉)

[1] Department of Chemistry, Korea Advanced Institute of Science and Technology (KAIST), 291 Daehak-ro, Yuseong-gu, Daejeon 34141, Republic of Korea
[2] Advanced Battery Center, KAIST Institute for NanoCentury, 291 Daehak-ro, Yuseong-gu, Daejeon 34141, Republic of Korea
[§] Vikram Singh and Soeun Kim contributed equally to this work.

ABSTRACT

Redox flow batteries (RFBs) are promising candidates to establish a grid-scale energy storage system for intermittent energy sources. While the current technology of vanadium RFBs has been widely exploited across the world, the rise in the price of vanadium and its limited volumetric energy density have necessitated the development of new kinds of redox active molecules. Organic molecules can be used as new and economical redox couples in RFBs to address these issues. In addition, the redox organic species also provide ample advantages to increase the voltage and solubility, provide multiple numbers of electron transfer, and ensure electrochemical/chemical stability by molecular engineering through simple synthetic methods. This review focuses on the recent developments in aqueous organic RFBs, including the molecular design and the corresponding cycling performance as these organic redox molecules are employed as either the negolyte or posolyte. Various strategies for tuning the electrochemical/chemical characteristics of organic molecules have improved their solubility, redox potential, cycling stability, and crossover issue across a separating membrane. We also put forward new strategies using nanotechnology and our perspective for the future development of this rapidly growing field.

1 Introduction

To reduce the use of fossil fuels, the evolution of energy conversion and storage technology is imperative [1–3]. A typical grid-scale energy storage system (ESS) is employed to store huge amounts of electricity in connection with the use of intermittent energy sources, and ESSs have been established in deserts and prairies all over the world [3–5]. In recent years, the development of ESSs can be promoted by the distribution of smart grids, and this has given birth to a new type of relatively compact ESS [3]. These ESSs have been installed in residential villages and commercial smart buildings to supply electricity for various purposes in daily life, such as charging electric vehicles, networks, and digital communications.

Since ESSs typically require a large scale and long-time operation with low maintenance, cost is one of the most important criteria [6]. In this light, lithium-ion batteries (LIBs) may not be an ideal candidate, because the material (e.g. lithium and non-aqueous electrolyte solution) and maintenance costs are quite high [7, 8]. Instead, aqueous solution-based redox flow batteries (RFBs) have been widely exploited as economical ESSs [9–13]. A vanadium RFB (VRFB) is the representative and commercial ESS, where four different charge states of vanadium, i.e. V^{2+}, V^{3+}, VO^{2+} and VO_2^{+}, are employed as the soluble and active redox species [14–16]. In strongly acidic solutions, V^{2+} and V^{3+} act as the negolyte, as indicated by the redox electrolyte providing relatively negative redox potential, and VO^{2+} and VO_2^{+} play a role of the posolyte that is in charge of relatively positive potential. The cell voltage of aqueous RFBs is limited from the potential window of water, which is a maximum of 1.6 V, with regard to the slow kinetics for electrolysis. Accordingly, the gravimetric and volumetric energy densities of VRFBs are low,

ca. 20–35 Wh·kg^{-1} and < 50 Wh·L^{-1}, which are more than 4-fold and 8-fold lower than those of LIBs, respectively (Fig. 1(a)) [17–19]. To enhance the overall storage amount in RFBs, large volume tanks containing the negolyte and posolyte with high concentrations are necessary, and each electrolyte solution in the tank is circulated to stacked carbon electrodes by using pumps (Fig. 1(b)). The increasing concentration of active redox species and the enlarging volume of negolyte/posolyte solution are proportional to the total energy density. In addition, separating the soluble redox active species from the conducting carbon electrode gives benefits for decoupling energy and power densities and easy system maintenance. However, the rise in the cost of vanadium and the limited volumetric energy density from VRFBs have motivated researchers to develop new kinds of redox active molecules. The alternative RFBs using Zn-Br show higher energy density owing to a larger operating voltage than VRFBs [20, 21]. In recent years, a redox couple of I^-/I_3^- has been suggested to be replaced with Br^-/Br_2 caused by its higher solubility [22, 23]. However, protection of cell component for these corrosive redox couples should be required [24].

These issues can be ameliorated by using organic molecules as new redox couples in RFBs [10, 25, 26]. The sources of organic molecules are abundant in the earth's crust and environmentally benign. This renders organic molecules to be potentially low cost with easy scalability [9]. The organic redox species also provide ample advantages for molecular engineering to increase solubility and voltage, provide multiple numbers of electron transfer, and ensure electrochemical/chemical stability via simple and economical synthetic methods [27–29]. Accordingly, electrochemical characteristics including reaction rate, diffusion coefficient, cell voltage, capacity, and cycling stability are highly designable due to ample structural

Address correspondence to hrbyon@kaist.ac.kr
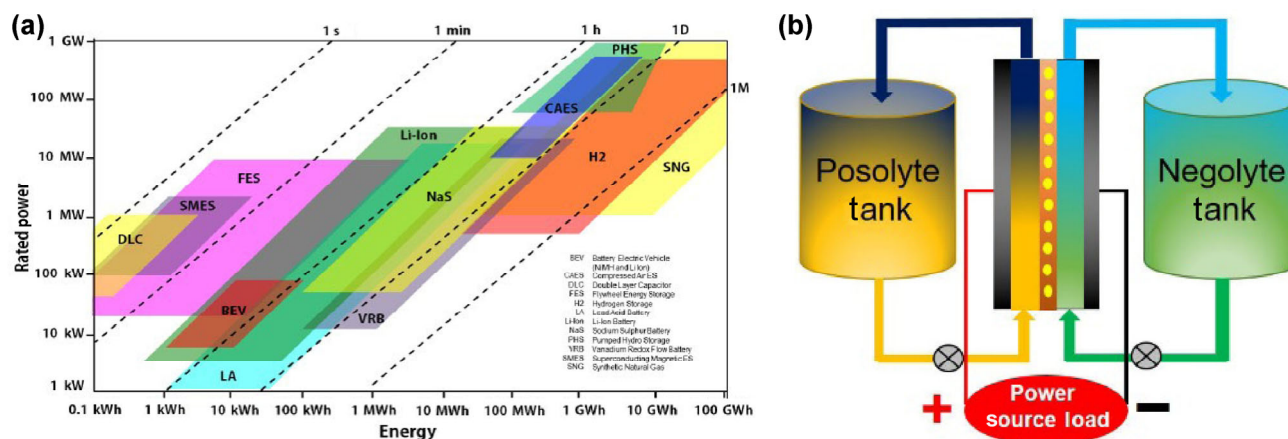
Figure 1 Energy density and cell configuration of RFB. (a) Comparison of energy densities and rate powers for various energy storages. (b) Schematic illustration of cell configuration of RFB. Reproduced with permission from Ref. [19], © Scientific & Academic Publishing Co. 2016.

diversity and tunability, which is a powerful advantage to enhance the energy and power density of organic RFBs [27, 28]. Therefore, organic RFBs are proposed to be promising prospects for assembling viable and clean energy-storage systems. Recently, research to design organic redox species and apply them to aqueous and non-aqueous RFBs has been intensively carried out. The well-known redox mediators such as quinone, anthraquinone, viologens, alloxazine, and 2,2,6,6-tetramethylpiperidin-1-yl)oxyl (TEMPO) have been preferentially investigated at this nascent stage, and their redox potential, solubility, and chemical stability have been adjusted by additional molecular engineering. This review paper focuses on various approaches for molecular tuning of organic negolytes and posolytes in aqueous medium, and provides an outlook for the future developing directions of organic RFBs using nanotechnology, while we note that non-aqueous-based systems have been previously reviewed [30].

2 Guidelines for design of organic redox species in RFBs

The performance of RFBs is mainly determined by their energy density and cycling stability. The theoretical energy density, which indicates the amount of charge stored, is calculated from the following Eq. (1) [24]

$$\text{Energy density (Wh·L}^{-1}) = nCFV/\mu_v \qquad (1)$$

where n is the number of electrons that participate in the redox reaction, C is the lower concentration of the redox-active materials from either the negolyte or catholyte (or either one if the concentration is same) with a unit of mol/L, F is the Faraday constant, V is the cell voltage, and μ_v is the reduced volume factor and is equal to the 1 + (max concentration of less soluble electrolyte)/(max concentration of more soluble electrolyte). This equation explicitly shows three core parameters of (1) cell voltage, (2) solubility, and (3) multiple electron transfer, which governs the functioning of RFBs.

The cell voltage is defined as the redox potential difference between the posolyte and the negolyte. Namely, higher cell voltage can be obtained from more negative redox potential of the negolyte and a more positive posolyte. The shift of the redox potential can be controlled by the design of organic redox species, where the addition of electron-donating groups (e.g. hydroxyl) and electron-withdrawing groups (e.g. sulfonic acid) move the potential to the negative (backward) and positive (forward) direction, respectively [31, 32]. The redox potentials of both posolyte and negolyte should reside in the range of stable aqueous solution, otherwise severe oxygen evolution reaction (OER) or hydrogen evolution reaction (HER) takes place.

The computational method can significantly aid in estimating potential shifts of redox couples with the introduction of functional groups [33–35]. Density functional theory (DFT) calculations allow us to compute the lowest unoccupied molecular orbital (LUMO) and highest occupied molecular orbital (HOMO) energy levels, solvation free energies, molecular solubility, and thermochemical stability. Recently, the Guzik group succeeded in screening 300 quinone derivatives, and predicted their redox potential values, positional effects of substituting groups as well as the structure-property relationships using high-throughput computational method [35]. By comparison with accessible experimental results, the computational methods should be developed further to reduce deviations from true redox potential. Representatively, the ion pairing of redox couple with surrounding electrolytes should be considered, which might otherwise make pronounced deviation from experimental results [36].

To raise the solubility, an ionic or hydrophilic moiety has generally been introduced to the redox organic species in the given pH of an aqueous solution. Methyl viologen and 4-OH-TEMPO have high solubility (2–3 M) in water. Whereas such high solubility decreases in a neutral electrolyte solution, the addition of bulky ammonium cations enhances the soluble concentration and electrochemical reaction rate. Since quinone and anthraquinone have low solubility at neutral pH, acidic and alkaline solutions are preferred. The charged and hydrophilic functionalities are decorated according to the pH of the electrolyte solution. In an acidic solution, the tethering sulfonic acid group increases the solubility through hydrogen bonding. However, much larger enhancement of solubility can be obtained in an alkaline solution where the sulfonate group and oxyanion group from the hydroxyl functional group allow the redox organics species to have a negative charge. As a prominent example, 2,5-dihydroxy-1,4-benzoquinone shows > 8 M solubility in KOH(aq) [37].

The number of electrons (e⁻) transferred significantly determine the energy density. Fast 2e⁻ transfer of quinone and anthraquinone at a single step is well known in acid and alkaline solutions [38]. Viologen shows stepwise 2e⁻ transfer [39]. However, the second redox reaction is generally not reversible due to instability and low solubility of the second reduction product. Recently, stable and continuous 2e⁻ transfer was demonstrated by implementing extended π-conjugation [40–42]. It is noted that the total molecular weight of organic redox species increases at the expense of grafting functional groups. Therefore, the balance of molecular mass and other factors should be considered to design optimum redox organic species and their application to RFBs [9].

The cycling stability has garnered significant attention with respect to organic RFBs, and is influenced by (1) electrochemical/chemical stability and (2) crossover of redox species. The chemical instability

after redox events is a crucial challenge for organic redox species, and it apparently appears with high concentration of redox species. The EC reaction, i.e. the electrochemical reaction followed by chemical reactions, yields an undesired product via an irreversible reaction, and the loss of redox species results in capacity fading in RFBs [43, 44]. For example, the Michael addition of water takes place at unsubstituted positions of quinone derivatives. Alloxazine easily decomposes via hydrolysis [21] and 4-OH-TEMPO can be self-oxidized [44] via hydroxyl radicals. The cathodic radical form of viologens undergoes dimerization and disproportionation [24]. To mitigate these undesired reactions, new functional moieties providing extended π-conjugation or the protection of highly reactive sites from a bulk structure have been introduced. The crossover of the redox couple is the other pivotal reason for capacity fading and also self-discharging. Although the negolyte and posolyte should be conceptually separated by a porous membrane, the smaller sized organic species can pass through the larger pores of the membrane. The implementation of an ion-exchange membrane and decoration of redox organic species with negative or positive charge can mitigate the crossover issue. The addition of a polymer backbone also has been widely applied to tie up organic redox species and increase the total size of redox species. Details of research approaches for the widely studied organic redox species are provided in the following sections.

3 Organic redox couples for aqueous RFBs

3.1 Quinone-based negolyte and hydroquinone-based posolyte

Quinones are classified as carbonyl-based (C=O) redox-active molecules with aromatic compounds, which show conjugated cyclic structures. The enolization of the carbonyl group through cathodic reactions stabilizes the anionic species of oxyanion by delocalization of accepted electrons over the conjugated structure. Quinones are biologically active molecules, forming redox-active centers and facilitating electron transfer, and are applied for photosynthesis and aerobic respiration/ATP synthesis [45, 46].

Quinones are well-known redox active molecules having high electrochemical reversibility and fast reaction rates. In particular, 2e$^-$ transfer generally takes place in a single step caused by the fast proton-coupled electron transfer (PCET) and the small activation energy to reorganize the aromatic ring through an outer-sphere electron transfer reaction [38]. In aqueous acidic solutions where the proton concentration is greater than the concentration of quinone, a single step of PCET produces dihydroquinone (Fig. 2(a)). However, if the concentration of quinone is higher than that of the protons (e.g. neutral pH), two steps of 1e$^-$ transfer take place stepwise. In alkaline solutions, oxyanions are preferentially formed through a single step of 2e$^-$ transfer. In this case where PCET does not occur, the oxyanions are strongly stabilized by the surrounding water molecules via hydrogen bonding, which may simultaneously lead to fast 2e$^-$ transfer (Fig. 2(a)) [38]. Quinones used in aqueous RFBs are summarized in Fig. 2(b) and Table 1.

The benzoquinone (e.g., 1,4-BZQ, **1a**) and its reduced form of hydroquinone (i.e. dihydoxybenzene, **1a'**) are the simplest form of quinones (Fig. 2(b)). The 1,4-BZQ (**1a**) has the reversible redox potential at around 0.6 V vs. the standard hydrogen electrode (SHE). However, the solubility is quite low at ~ 0.1 M in a neutral pH aqueous solution. The Yu group demonstrated a reasonable diffusion coefficient of 1,4-BZQ at 8.8×10^{-6} cm^2·s^{-1} in 0.2 M Li$_2$SO$_4$(aq) [48]. In particular, the reaction rate constant was estimated as 2.0×10^{-3} cm·s^{-1}, which is faster than that of the redox species VO$_2^+$/VO^{2+} and Br$_2$/Br$^-$ employed in commercial RFBs. With increasing pH, the solubility of 1,4-BZQ rises and reaches > 1 M at pH = 9, which
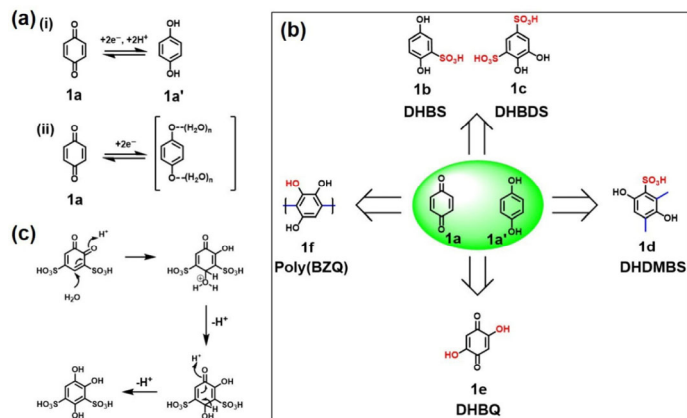
Figure 2 Electrochemical and chemical reactions of quinone and hydroquinone derivatives. (a) Electrochemical reaction processes of 1,4-BZQ in (i) acidic and buffer solution and (ii) unbuffered and alkaline solution. Readapted with permission from Ref. [38], © American Chemical Society 2007. (b) Various molecular designs of quinone and hydroquinone. (c) Michael addition process of water to unsubstituted sites in the anodic form of **1c** [47]. Readapted with permission from Ref. [47], © Hoober-Burkhardt, L. et al. 2017.

provides potential to enhance the energy density in RFBs. The Cao group introduced sulfonic acid groups to two quinols, 1,4-dihydroxybenzene-2-sulfonic acid (DHBS, **1b**, Fig. 2(b)) and 1,2-dihydroxybenzene-3,5-disulfonic acid (DHBDS, **1c**, Fig. 2(b)) [49]. The sulfonic acid groups enhanced the solubility to 0.2 M for DHBS in an acidic solution and shifted the redox potential to 0.71 and 0.72 V vs. SHE for DHBS and DHBDS, respectively. As the posolyte in 3 M H$_2$SO$_4$(aq), DHBS showed stable redox behavior, ~ 99% coulombic efficiency (CE) and ~ 70% energy efficiency (EE) over 100 cycles with the negolyte of PbSO$_4$/Pb. By contrast, DHBDS was subject to nucleophilic addition of water after anodic reaction (Fig. 2(c)). This Michael addition resulted in hydroxylation to the 4-position of DHBDS, yielding 1,2,4-trihydroxybenzene-3,5-disulfonic acid and 1,2,4,6-tetrahydroxybenzene-3,5-disulfonic acid [47]. The Narayanan group also observed similar Michael addition of water from DHBDS [47, 50]. To mitigate this undesired reaction, they employed 3,6-dihydroxy-2,4-dimethylbenzenesulfonic acid (DHDMBS, **1d**, Fig. 2(b)), which has only a single unsubstituted position at the position of 5 [50]. With a 9,10-anthraquinone-2,7-disulfonic acid as the negolyte, the capacity fading rate was measured as ~ 0.05%/cycle over 25 cycles with 98% CE. The crossover of small-size DHDMBS through a Nafion membrane was the main cause of capacity fading. However, these initial studies of acidic solution-based RFBs typically showed severe capacity loss, low energy density, and a high IR drop at high current density.

The solubility of BZQ derivatives could considerably rise with increasing pH. Additional hydroxyl groups grafted to unsubstituted positions of BZQ further enhance the molecular solubility. Importantly, these electron-donating groups can shift the redox potential more negatively, and thus these quinone derivatives can act as promising negolytes in RFBs. The Aziz group fabricated an alkaline RFB comprising 2,5-dihydroxy-1,4-benzoquinone (DHBQ, **1e**, Fig. 2(b)) as the negolyte along with a posolyte of K$_4$Fe(CN)$_6$ [37]. The DHBQ showed > 8 M solubility and a cathodic potential of –0.72 V vs. SHE in 1 M KOH(aq), which was in line with a cell voltage of 1.21 V in RFBs. However, since the crossover of small DHBQ across a Nafion 115 membrane reduced the capacity, it is necessary to increase the size of DHBQ. The full blocking of unsubstituted sites of DHBQ could be one of the solutions, which may also mitigate the Michael addition of water. However, the result of fully substituted DHBQ, such as 3,6-bis(diphenylmethyl)-2,5-dihydroxy-1,4-benzoquinone (DPM-DHBQ), showed large peak separation (ΔE_{pp} = ~ 500 mV), sluggish reaction kinetics, and low solubility

Table 1 A summary of relevant quinone and anthraquinone derivatives used in aqueous RFBs along with their electrochemical properties

Quinones, anthraquinones and derivatives	Negolyte/ posolyte	Solubility in water	Potential/cell potential	Supporting electrolyte	Capacity retention	CE, EE	k_0 (cm·s^{-1}), D (cm^2·s^{-1})	Cell cycle number
1b	AQS (2a) or AQDS (2b)	Max 0.8 M in 1 M H_2SO_4	0.7 V (vs. SHE)	1 M H_2SO_4	N/A	N/A	5.52×10^{-4} cm·s^{-1}, 4.28×10^{-6} cm^2·s^{-1}	N/A
1c	AQS (2a) or AQDS (2b)	Max 1 M in 1 M H_2SO_4	0.87 V (vs. SHE)	1 M H_2SO_4	> 90%	N/A	1.55×10^{-4} cm·s^{-1}, 3.80×10^{-6} cm^2·s^{-1}	12
1d	AQDS (2b)	Max 2 M in 1 M H_2SO_4	0.82 V (vs. NHE)	1 M H_2SO_4	99.95% per cycle	0.1 A·cm^{-2} > 98%, N/A	1.30×10^{-4} cm·s^{-1}, 4.12×10^{-6} cm^2·s^{-1}	25
1e	Fe(CN)$_6^{4-}$	> 8 M in 1 M KOH	−0.72 V (vs. SHE)/1.21 V	1 M KOH	99.76% per cycle	0.1 A·cm^{-2} 99%, 65%	2.12×10^{-3} cm·s^{-1}, 3.66×10^{-6} cm^2·s^{-1}	150
1f	K$_3$Fe(CN)$_6$/ K$_4$Fe(CN)$_6$	N/A	N/A	1 M KOH	99.96% per cycle	10 mA·cm^{-2} 99.962%, 37%	N/A	400
2b	HBr/Br$_2$	> 1 M (pH = 0)	0.21 V (vs. SHE)	1 M H_2SO_4	> 99% per cycle	N/A	7.2×10^{-3} cm·s^{-1}, 8×10^{-6} cm^2·s^{-1}	10–15
2c	HBr/Br$_2$	> 1 M	0.19 V (vs. SHE)	2 M H_2SO_4	Poor	N/A	1.56×10^{-2} cm·s^{-1}	15
2e	Fe(CN)$_6^{4-}$	> 0.6 M in 1 M KOH	−0.7 V (vs. SHE)	1 M KOH	99.9% per cycle	0.1 A·cm^{-2} 99%, 84%	N/A	100
2h	Fe(CN)$_6^{4-}$	> 1 M (pH = 14)	−0.52 V (vs. SHE)	1.2 M KOH	99.999% per cycle	50 mA·cm^{-2} > 99%, 88%	5.26×10^{-13} cm^2·s^{-1}	250

due to the effects of bulky aromatic rings [37]. Alternatively, the polymerization of BZQ (poly(BZQ), **1f**, Fig. 2(b)) was proposed. Along with a posolyte of K$_3$Fe(CN)$_6$/K$_4$Fe(CN)$_6$, the poly(BZQ)-based RFB displayed ~ 0.04%/cycle capacity fading over 300 cycles after stabilization. The CE fluctuated at the initial 100 cycles while it stabilized in the following 300 cycles with 99.962% of the CE. However, the measured capacity is only ~ 25% of the theoretical value and the EE is only ~ 37%, indicating a detrimental effect of large size and coiled nature of the polymeric backbone.

Naphthoquinone (NQ) has lower solubility than BZQ, which is ~ 0.02 M in water. The Bentien group showed that 2-hydroxy-1,4-naphthoquinone (HNQ), a naturally existing red-orange dye, is modestly soluble in 0.48 M in alkaline solution and could be used as the negolyte in RFBs with a potential of −0.50 vs. SHE [51]. A RFB based on HNQ displayed very fast capacity decay, presenting almost ~ 50% capacity retention per cycle. This result was attributed to the Michael addition of water at the unsubstituted sites of HNQ. The Jin group reported a new NQ derivative of 2-hydroxy-3-carboxy-1,4-naphthoquinone (HCNQ). The negative charge of the carboxylate group in an alkaline solution increases the solubility up

to 1.2 M [52]. The redox potential is measured to −0.53V vs. SHE. The authors claimed that the slightly negative potential of HCNQ compared to that of HNQ is attributable to the nullified effect of the carboxylate group, as the electron-withdrawing characteristics of the carboxylate group are involved in the π-conjugation of the NQ structure. The RFBs consisting of 0.5 M HCNQ negolyte ‖ a Nafion membrane ‖ 0.4 M K$_4$Fe(CN)$_6$ posolyte in a strong alkaline solution (pH = 14) showed a cell voltage of ~ 1.02 V. The initial discharge was delivered to a capacity of 18.8 Ah·L^{-1} at a high current density of 100 mA·cm^{-2}, which was ~ 70% of the theoretical capacity. The capacity retention was 94.7% over 100 cycles and converted to a capacity fading rate of 3.4% per day. When the negolyte concentration was doubled to 1.0 M, the capacity fading rate increased to 6.4% per day due to the EC reaction of HCNQ.

In all, quinone and BZQ derivatives are attractive as the redox couple in aqueous RFBs owing to their fast, single-step 2e$^-$ transfer and remarkable solubility in alkaline solutions. The small size of the redox couple is the main reason for crossover-related issues leading to unsatisfied cycling performance, which has been alleviated by designing oligometric quinone derivatives.
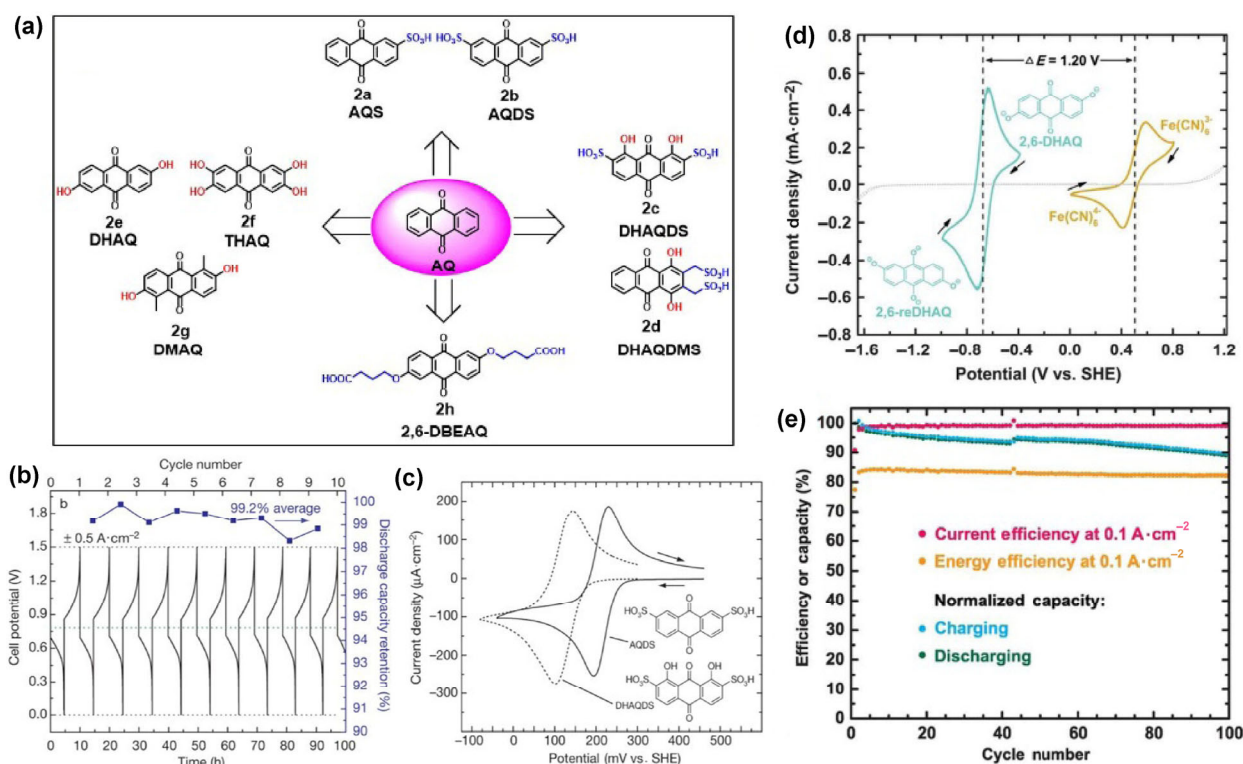
3.2 Anthraquinone-based negolyte

Anthraquinones (AQs) are polycyclic aromatic hydrocarbons having extended π-conjugated structures, which render high chemical stability and negative redox potential. The fully delocalized electrons in the AQ body reduce the possibility of Michael addition. In addition, the large size of AQ reduces the chance of crossover through membranes. The well-established synthetic methods enable us to add various functional groups, which increases the solubility of AQ. Furthermore, the fast and reversible 2-electron transfer process with the aid of PCET is applied for AQ electrochemistry, in a similar manner to BZQ. Thanks to these diverse advantages, many RFB studies have used AQ as the negolyte and various molecular engineering studies have been progressed (Table 1).

The Aziz group compared two negolytes of 9,10-anthraquinone-2-sulfonic acid (AQS, **2a**, Fig. 3(a)) [53] and 9,10-anthraquinone-2,7-disulfonic acid (AQDS, **2b**, Fig. 3(a)) in an acidic solution [54]. The sulfonic acid groups imparted hydrophilicity and raised the solubility of AQS and AQDS to ~ 1 M at pH = 0. The reaction rate of AQDS was 7.2×10^{-3} cm·s^{-1}, comparable to that of BZQ. In the acidic RFBs including the posolyte of Br$_2$/Br$^-$, both negolytes showed comparable cycling performance. For the AQDS-based RFB case, the capacity retention was > 99% per cycle and the volumetric energy density was projected to 50 Wh·L^{-1} (Fig. 3(b)). The AQS having a single sulfonic group showed a more negative redox potential than AQDS with two electron-withdrawing sulfonic groups, which led to the AQS-based RFBs having higher open circuit voltage (OCV). In addition, its smaller molecular size enhanced the power density. The addition of electron-donating hydroxyl groups to AQDS to make 1,8-dihydroxy-9,10-anthraquinone-2,7-disulfonic acid (DHAQDS, **2c**, Fig. 3(a)) could negatively shift the potential to 100 mV (Fig. 3(c)), which extended the cell voltage by 11% in RFBs. In addition, hydrogen bonding between the hydroxyl and the neighboring keto

groups in DHAQDS improved the k_0 value for the cathodic reaction to 1.56×10^{-2} cm·s^{-1}. However, since the anodic kinetics is quite sluggish, the DHAQDS-based RFBs only could be performed at low current density. Further, the crossover of Br$_2$ posolyte was significant. The unintended reaction between Br$_2$/Br$^-$ and the sulfonic acid groups in DHAQDS also led to considerable capacity fading. The same stoichiometry but the asymmetric molecular structure of 1,4-dihydroxyanthraquinone-2,3-dimethylsulfonic acid (DHAQDMS, **2d**, Fig. 3(a)) suppressed the Br substitution even if the crossover of Br$_2$ took place [53]. Nevertheless, the cycling performance with DHAQDMS was worse than DHAQDS, as the reduced form of DHAQDMS was chemically unstable. Presumably, the loss of conjugation between the sulfonic acid groups and the AQ backbone after the cathodic reaction triggers chemical decomposition.

The Armand group also designed two isomers of dihydroxy-AQ dyes such as quinizarin (1,4-dihydroxyanthraquinone) and alizarin (1,2-dihydroxyanthraquinone), which are only sparingly soluble (~ 0.004 M) in neutral pH and acidic aqueous solutions due to π-stacking and intermolecular hydrogen bonds [55]. The addition of the sulfonate group with counter cations, such as tetrakis(hydroxyethyl)-ammonium (TKEN) and tetrakis(hydroxymethyl)-phosphonium (TKMP), raised their solubilities. The quinizarin derivatives displayed two reversible redox peaks, $E_{1/2} = 0$ and 1.0 V vs. SHE with 0.4 M solubility in an acidic solution, which suggested the potential application of all quinizarin RFB; namely, the quinizarin can be exploited as both the negolyte and anolyte in a RFB. Alizarin-TKEN presented a single redox peak at $E_{1/2} = -0.2$ V and a maximum solubility of 1.6 M, showing the highest solubility in an acidic condition.

The alkaline RFB could surmount the above-mentioned challenges arising in the acidic electrolyte solution. The hydroxyl group itself fully raises the solubility of AQ and moves the redox potential more negatively. The Aziz group tested the simple AQ form of

Figure 3 Electrochemical reactions of anthraquinone as the negolyte in aqueous RFBs. (a) Various molecular designs of anthraquinone. (b) Cycling performance of aqueous RFB with 1 M **2b** (1 M H$_2$SO$_4$) ‖ 0.5 M Br$_2$/3 M Br$^-$ at a current density of 0.5 A·cm^{-2}. (c) Comparison of cyclic voltammograms of **2b** and **2c** in acidic solution. (d) Cyclic voltammograms of **2e** (dark cyan) and K$_4$Fe(CN)$_6$ (gold) in 1 M KOH(aq). (e) Cycling performance of aqueous RFB with **2e** ‖ K$_4$Fe(CN)$_6$ at 0.1 A·cm^{-2}. (b) and (c) are reproduced with permission from Ref. [54], © Springer Nature Publishing AG 2018. (d) and (e) are reproduced with permission from Ref. [56], © American Association for the Advancement of Science 2018.

2,6-dihydroxyanthraquinone (DHAQ, **2e**, Fig. 3(a)) and confirmed a redox potential of –0.69 V vs. SHE and > 0.6 M solubility at pH > 12 (Fig. 3(d)) [56]. Along with the posolyte of 0.4 M $K_4Fe(CN)_6$, the 0.5 M DHAQ-based RFBs showed 0.1% capacity fading per cycle with CE > 99% and EE > 84% at a current density of 0.1 A·cm^{-2}, and 5% per day (Fig. 3(e)). The authors indicated that the capacity loss is more likely due to the leakage of the electrolyte solution rather than the crossover of negolyte and/or posolyte. The power density of a DHAQ-based RFB was ~ 0.45 W·cm^{-2} at 20 °C and ~ 0.7 W·cm^{-2} at 45 °C, which was associated with the cell area specific resistance (ASR) of 0.560 and 0.878 Ω·cm^{-2}, respectively. The difference in the ASR with respect to temperature is mostly determined from the diffusion of DHAQ in the Nafion membrane. It is also noted that the negative charge of the sulfonate group is expressed in the Nafion membrane in the alkaline solution. Further substitutions of DHAQ to yield 2,3,6,7-tetrahydroxyanthraquinone (THAQ, **2f**, Fig. 3(a)) and 1,5-dimethyl-2,6-dihydroxyanthraquinone (DMAQ, **2g**, Fig. 3(a)) lower the cathodic potential to –0.82 V, leading to a cell voltage of ~ 1.35 V with the posolyte of $K_4Fe(CN)_6$. Recently, the Aziz group developed 4,4'-((9,10-anthraquinone-2,6-diyl)dioxy)dibutyrate (2,6-DBEAQ, **2h**, Fig. 3(a)). The alkyl chains and terminal carboxylate groups showed six-fold increased solubility, 0.6 M at pH = 12 and 1 M at pH = 14 [57]. The theoretical volumetric energy density could be calculated as 17 Wh·L^{-1} when $K_4Fe(CN)_6/K_3Fe(CN)_6$ is used as the posolyte. Such high energy density can fulfill the techno-economic criteria of RFBs. These 0.5 M 2,6-DBEAQ-based RFBs with a symmetric configuration showed superb cycling performance; a capacity fading rate of < 0.001% per cycle and < 0.01% per day. They also compared 2,6-DBEAQ with two structural isomers, 1,2-DBEAQ and 1,8-DBEAQ. The symmetric flow cells using these isomers, however, exhibited far more rapid capacity fading, ~ 0.1% per cycle and ~ 10% per day. The authors suggested that these isomers were susceptible to γ-hydroxybutyrate cleavage in the presence of hydroxide ions and water.

The RFB performance was also determined from various membranes.

Significant capacity fading was observed from a perfluorosulfonic acid (PFSA) membrane due to the severe crossover of redox species, while the crossover was significantly suppressed by the non-fluorinated E-600 series' membrane. The non-fluorinated membrane revealed remarkably low permeabilities for 2,6-DBEAQ (ca. 5.26 × 10^{-13} cm^2·s^{-1}) and also $[Fe(CN)_6]^{3-}$ (ca. 4.4 × 10^{-12} cm^2·s^{-1}), which were at least one order of magnitude lower than the Nafion 212 membrane. The low ASR of the E-600 membrane, ~ 1 Ω·cm^2 in 1 M KOH(aq), contributed to a high power density of 0.24 W·cm^{-2} in 2,6-DBEAQ-based RFBs.

In summary, AQs, consisting of a π-conjugated structure, have high chemical stability and fast electron transfer kinetics. Notably, side reactions such as Michael addition can be significantly suppressed. The solubility of AQ derivatives has been improved by design of AQ. Representatively, the addition of hydroxyl groups can enhance the solubility of AQs in alkaline solution, and also shift the redox potential towards negative direction. Along with the help of computational simulations [39, 40], various AQ derivatives have been suggested, which can endow AQs as the promising negolyte for organic RFBs.

3.3 Viologen-based negolyte

Viologen (Vi^{2+}), referring to 1,1'-disubstituted 4,4'-bipyridinium ions, is another promising candidate for negolytes in aqueous RFBs. Vi^{2+} has been widely utilized as redox-mediators and redox-indicators owing to its electrochemical reversibility along with color change [39, 58]. The simplest viologen form of methyl viologen (referring to 4,4-dimethyl bipyridinium dichloride, MVi^{2+}, **3a**, Fig. 4(a)) has > 3 M solubility in water, and shows stepwise two electron transfer (Fig. 4(b)). The dication of MVi^{2+} is first reduced to the radical cation of MVi$^+$ via 1e$^-$ transfer. This cathodic reaction is fast ($k_0 = 2.8 × 10^{-4}$ cm·s^{-1}) and highly reversible at –0.45 V vs. SHE. The radical cation MVi$^+$ is quite stable in an aqueous solution because the unpaired electron is delocalized throughout the main body of bipyridine. The second reduction step produces the non-ionic MVi^0
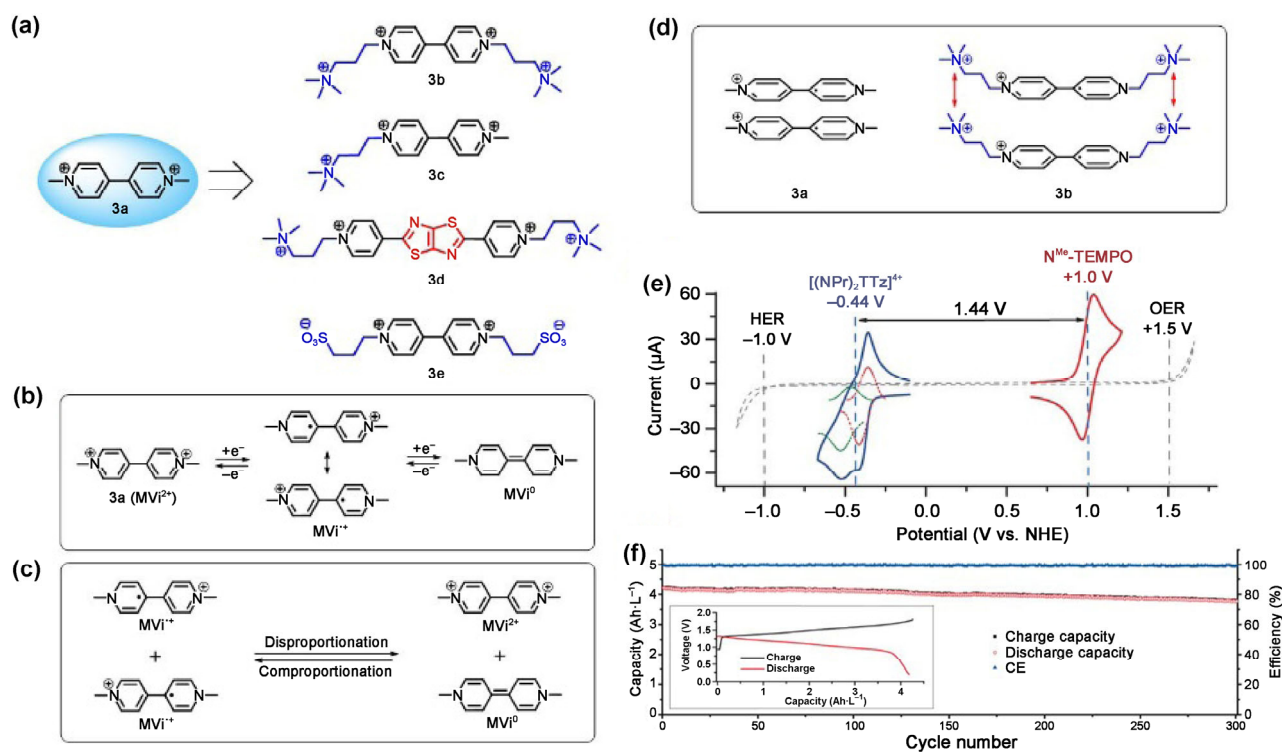
Figure 4 Electrochemical and chemical reactions of viologen as the negolyte in aqueous RFBs. (a) Various molecular designs of viologen. (b) Two steps of electrochemical reaction process. (c) Undesired chemical reactions from the cathodic forms of viologens. (d) Illustration of the strategy to suppress dimerization of viologens. (e) Cyclic voltammograms of **3d** (blue) and 4-TMA$^+$-TEMPO (red) in 0.5 M NaCl (aq). (f) Cycling performance of aqueous RFB with 0.1 M **3d** || 0.2 M 4-TMA$^+$-TEMPO (**5c**) at 0.1 A·cm^{-2}. (e) and (f) are reproduced with permission from Ref. [41], © Wiley-VCH Verlag GmbH & Co. KGaA, Weinheim 2017.

molecule at –0.76 V vs. SHE, while this electrochemical process is not very reversible due to the low solubility of MVi^0. Since the electrochemical process of Vi^{2+} is independent of pH, most studies have achieved the reversible first e^- transfer step and these negolytes were utilized to develop neutral RFBs.

The Wang group examined the performance of neutral RFBs combining 0.5 M MVi^{2+} negolyte and 4-OH-TEMPO posolyte with 1 M NaCl(aq). This RFB offered a cell voltage of 1.25 V and stable charge–discharge performance over 100 cycles with ~ 100% CE [59]. The Liu group also demonstrated long-time cycling performance of 0.5 M MVi^{2+}-based RFB with the posolyte of (ferrocenylmethyl)trimethylammonium chloride ($FcTMA^+Cl^-$), showing a capacity retention of 91% over 700 cycles, which converts to 0.01% capacity fading rate per cycle [24]. It is noteworthy that the reported RFB tests were mostly carried out with low concentrations of MVi^{2+}. At higher concentrations, the EC reaction between MVi^{+} molecules forms a dimer that occasionally undergoes disproportionation ($2MVi^{+} \rightarrow MVi^{2+} + MVi^0$, Fig. 4(c)). Therefore, the re-oxidized MVi^{2+} is fed again during the charging process while the insoluble MVi^0 causes capacity loss [60]. Indeed, the same RFB with higher concentration (0.7 M) delivered a capacity retention of 81% over 500 cycles, which is equivalent to 0.04% capacity loss rate per cycle.

To suppress such dimerization and disproportionation from the viologen radicals Vi^{+}, the Aziz group suggested the addition of two quaternary ammonium groups to bipyridiniums. This bis(3-trimethylammonio)propyl viologen tetrachloride ($BTMAP^{2+}$-Vi^{2+}, **3b,** Fig. 4(a)) has a total +4 charge, thereby allowing significant electrostatic repulsion between $BTMAP^{2+}$-Vi^{+} molecules during the charging process and the suppression of dimerization (Fig. 4(d)) [60]. The solubility of $BTMAP^{2+}$-Vi^{2+} is ~ 2.0 M, and the reaction rate (0.22 × 10^{-1} cm·s^{-1}) is two orders of magnitude higher than that of MVi^{2+}. In the proof-of-concept RFB tests, 1.3 M $BTMAP^{2+}$-Vi^{2+} coupled with the same concentration of bis((3-trimethylammonio)propyl)ferrocene dichloride ($BTMAP^{2+}$-Fc) posolyte showed a cell voltage of 0.75 V and retained a capacity of 98.58% over 250 cycles, i.e. 0.0057% capacity fading per cycle and 0.10% per day. This capacity retention is ~ 40-fold higher than the capacity obtained exploiting 0.7 M MVi^{2+} negolyte. The Liu group also confirmed highly stable 0.5 M $BTMAP^{2+}$-Vi^{2+} with a counterpart of 0.5 M 4-trimethylammonium-TEMPO (4-TMA$^+$-TEMPO) [18]. A total cell voltage was increased to 1.38 V by using a TEMPO-based posolyte, and the capacity retention was measured as 97.48% over 500 cycles, indicating ~ 0.005% fading per cycle.

To vitalize the second reduction step of Vi^{2+}, which raises the total energy density two-fold in RFBs, essential studies to increase the solubility of Vi^0 have been carried out. The Liu group designed a $2e^-$ storage negolyte by functionalization with a single TMAP$^+$, namely 1-methyl-1'-[3-(trimethylammonio)propyl]-4,4'-bipyridinium trichloride ($MTMAP^+$-Vi^{2+}, **3c,** Fig. 4(a)) [42]. The rate constants for the first and second cathodic reactions of $MTMAP^+$-Vi^{2+} are comparable, 3.64 × 10^{-1} and 3.60 × 10^{-1} cm·s^{-1}, respectively, which are surprisingly three orders of magnitude higher than that of MVi^{2+}. The RFB containing 0.25 M $MTMAP^+$-Vi^{2+} coupled with 0.5 M FcNCl exhibited two obvious charge/discharge voltage plateaus at ~ 1.0 and 1.4 V, and the capacity retention was 91.39% over 50 cycles. Similar examinations were also carried out for $BTMAP^{2+}$-Vi^{2+} (**3b**) consisting of double TMAP$^+$ groups, which was previously tested as the $1e^-$ storage negolyte by the Aziz group [60]. The rate constant for the first cathodic reaction was measured as 3.09 × 10^{-1} cm·s^{-1}, which was more than one order of magnitude higher than that measured by the Aziz group [60]. The second cathodic rate reaction was identical to the first rate reaction at 3.05 × 10^{-1} cm·s^{-1}. The 0.25 M $BTMAP^{2+}$-Vi^{2+} delivered higher cycling stability than $MTMAP^+$-Vi^{2+}, ~ 99.00% capacity retention over 100 cycles. The resulting capacity

retention from the $2e^-$ storage negolyte of $BTMAP^{2+}$-Vi^{2+} is comparable to that from the $1e^-$ storage of the same molecule [60]. However, it should be noted that for the latter case for $1e^-$ storage, the concentration of $BTMAP^{2+}$-Vi^{2+} was ~ 1.3 M, more than five-fold higher than the former case. Therefore, further studies are needed to confirm the stability of $2e^-$ transfer at higher concentrations of the negolyte. Furthermore, the Liu group reported an extended π-conjugation of Vi^{2+} using a thiazolo[5,4-d]thiazole (TTz) group [41]. The central TTZ group is symmetrically linked with two pyridinium cations, and thus the enhanced resonance and electron delocalization stabilizes Vi^{+} and Vi^0. This 4,4'-(thiazolo[5,4-d]thiazole-2,5-diyl)bis(1-(3-(trimethylammonio)propyl)pyridine-1-ium) tetrachloride ($BTMAP^{2+}$-TTZ-Vi^{2+}, **3d**, Fig. 4(a)) acts as stable $2e^-$ storage for the negolyte. The terminal TMAP$^+$ groups render the solubility of $BTMAP^{2+}$-TTZ-Vi^{2+} to 1.3 M. The reaction kinetics of k_0 for the first cathodic reaction is 2.8 × 10^{-1} cm·s^{-1}. As a result, the neutral RFBs with 0.1 M $BTMAP^{2+}$-TTZ-Vi^{2+} and 0.2 M posolyte of 4-TMA$^+$-TEMPO (**5c**) showed a cell voltage of 1.44 V (Fig. 4(e)) and yielded 90% capacity retention after 300 cycles (Fig. 4(f)). Notably, the theoretical energy density of 1.3 M $BTMAP^{2+}$-TTZ-Vi^{2+} (53.7 Wh·L^{-1}) is higher than that from the $1e^-$ storage of 3 M MVi^{2+} (45.5 Wh·L^{-1}), which highlights the power of multiple electron transfer for improvement of the energy density.

The positive charge of viologen has typically required anion-exchange membranes to prevent the crossover issue. However, this implies that the negative charge of posolyte excludes the use of Vi^{2+} and anion-exchange membranes in the same RFB. The Liu group attached the negative charge of sulfonate functional group to Vi^{2+} and produced 1,1'-bis(3-sulfonatopropyl)-4,4'-bipyridinium ((SPr)$_2^{2-}$-Vi^{2+}, **3e**, Fig. 4(a)) [61]. The sulfonate groups at both ends of propyl chains enable (SPr)$_2^{2-}$-Vi^{2+} to have high solubility (~ 2 M) and hinder dimerization of (SPr)$_2^{2-}$-Vi^{+} via electrostatic repulsion. Furthermore, the crossover issue from (SPr)$_2^{2-}$-Vi^{2+} and (SPr)$_2^{2-}$-Vi^{+} is suppressed through cation-exchange Nafion membranes (a pore size of ~ 2.4 nm). This is attributed to both the large size of molecules and negative charged arms. As a result, RFBs including 0.5 M (SPr)$_2^{2-}$-Vi^{2+} and 2.0 M KI show a cell voltage of 1.0 V and 94.1% total capacity retention after 300 cycles with a Nafion membrane. From a Selemion CSO cation-exchange membrane that is ~ 5 times cheaper than Nafion, the comparable RFB performance of 98.8% total capacity retention after 100 cycles was also evaluated. The reported results are summarized in Table 2.
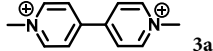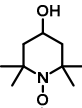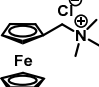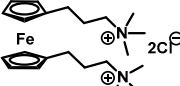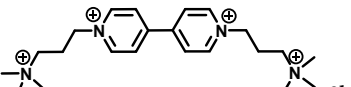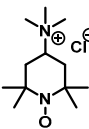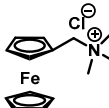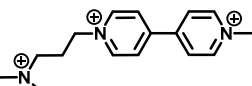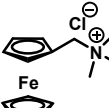
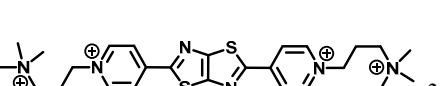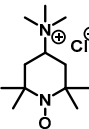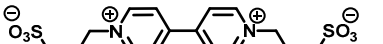Overall, the dication of MVi^{2+} has been suggested as a promising negolyte in neutral aqueous medium. The most significant challenge is low solubility of both MVi^{2+} and MVi^0 that is formed after $2e^-$ reduction. In particular, precipitation of MVi^0 is the central reason forcing MVi^{2+} to only $1e^-$ transfer. The cathodic form of MVi^{+} is stable in aqueous solution, while this radical cation exacerbates disproportionation and dimerization. Thus, designs of MVi^{2+} with anchoring charged substituents and attached π-conjugated frameworks have been attempted to enhance chemical stability and promote $2e^-$ transfer reaction, respectively. Such research progresses have shown a promise for the new class of negolyte applied for neutral RFBs, while further studies are needed to get increased solubility, longer cycling number [62] and stabilised $2e^-$ redox reactions.

3.4 Alloxazine-based negolyte

The alloxazine is the redox-active backbone of flavin mononucleotide (FMN) [63]. The simple synthetic method and reversible $1e^-$ electrochemical reaction allows alloxazine to be used as the negolyte. However, since the alloxazine is easily precipitated via π-stacking, [64] and participated in hydrolysis that forms redox-inactive species (Figs. 5(a) and 5(b)) [65], the hydrophilic functional groups should be decorated to improve the chemical stability in RFBs.

The Aziz group developed alloxazine functionalized with carboxylic

Table 2 A summary of viologen derivatives used in aqueous RFBs along with electrochemical properties

Viologens and derivatives	Posolytes	Solubility in water	Potential/cell potential	Capacity retention	CE, EE	k_0 (cm·s⁻¹) D (cm²·s⁻¹)
3a	(TEMPO-OH)	3.0 M	−0.45 V (vs. NHE)/1.25 V	0.5 M 89%, 100 cycles	60 mA·cm⁻² > 99%, 62.5%	2.8×10^{-4} 2.57×10^{-5}
	(ferrocenylmethyl ammonium)	3.5 M	−0.45 V (vs. NHE)/1.05 V	0.7 M 81%, 500 cycles	60 mA·cm⁻² > 99%, 65%	N/A
3b	(ferrocene diammonium, 2Cl⁻)	2.0 M	−0.36 V (vs. SHE)/0.75 V	1.3 M 98.58%, 250 cycles	50 mA·cm⁻² > 99.95%, > 65%	2.2×10^{-2} 3.3×10^{-6}
	(TEMPO ammonium, Cl⁻)	N/A	−0.38 V (vs. NHE)/1.38 V	0.5 M 97.48%, 500 cycles	60 mA·cm⁻² > 99%, 57.1%	N/A
	(ferrocene ammonium, Cl⁻)	1.8 M	−0.35, −0.72 V (vs. NHE)/ 0.95, 1.32 V	0.25 M 100 cycles	60 mA·cm⁻² > 99%, 59%	> 0.309/> 0.305 3.9×10^{-6}/ 3.8×10^{-6}
3c	(ferrocene ammonium, Cl⁻)	1.6 M	−0.39, −0.78 V (vs. NHE)/ 1.00 V, 1.38 V	0.25 M 91.4%, 50 cycles	60 mA·cm⁻² > 99%, 63%	> 0.364/> 0.360 5.4×10^{-6}/ 5.3×10^{-6}
3d	(TEMPO ammonium, Cl⁻)	1.3 M	−0.44 V (vs. NHE)/1.44 V	0.1 M 91.4%, 300 cycles	40 mA·cm⁻² > 99%, 70%	0.28 3.15×10^{-6}
3e	(I⁻)	2.0 M	−0.43 V (vs. NHE)/1.0 V	0.5 M 94.1%, 300 cycles	60 mA·cm⁻² > 99%, 58%	> 0.28 3.26×10^{-6}
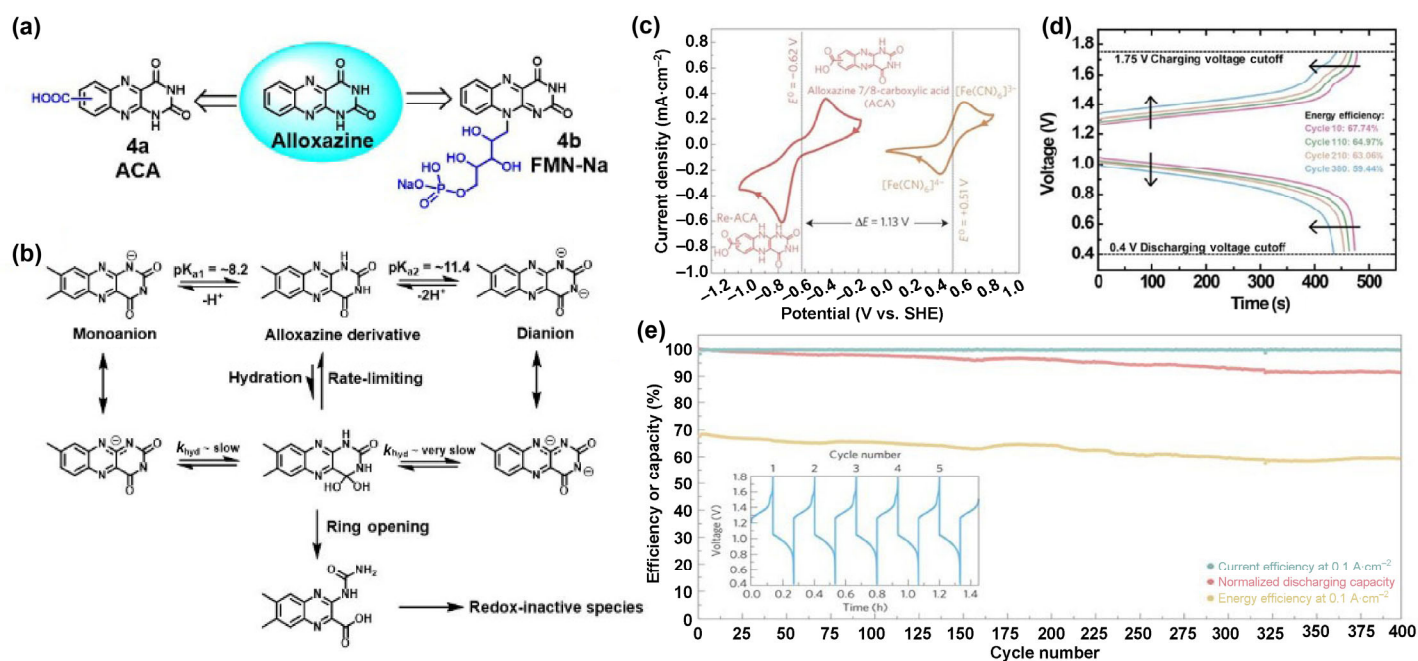
Figure 5 Electrochemical and chemical reactions of alloxazine as the negolyte in aqueous RFBs. (a) Two molecular designs of alloxazine. (b) Hydrolysis-triggered decomposition pathway. (c) Cyclic voltammogram of **4a** (red) and $K_4Fe(CN)_6$ (gold) in alkaline solution (pH =14). The sweeping rate was 100 mV·s⁻¹. (d) Galvanostatic charge-discharge profiles and (e) cycling performance of aqueous RFB with 2 mM **4a** ‖ 2 mM $K_4Fe(CN)_6$ at 100 mV·s⁻¹. The inset in (e) shows the voltage-time profile recorded between the first and fifth cycle. (b)–(e) are reproduced with permission from Ref. [65], © Springer Nature AG 2018.
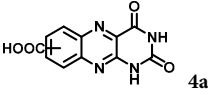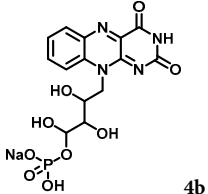
acid (ACA, **4a**, Fig. 5(a)), which showed a reduction potential of −0.60 V vs. SHE (Fig. 5(c)) and the reaction rate of ~ 1.2×10^{-5} cm·s^{-1} in an alkaline solution (pH = 14) [65]. They confirmed negligible chemical degradation in the alkaline solution for six weeks. The RFBs of 0.4 M ACA negolyte assembled with the posolyte of 0.4 M $K_4Fe(CN)_6$ + 40 mM $K_3Fe(CN)_6$ revealed a cell voltage of 1.2 V (Fig. 5(d)), a power density of 0.35 W·cm^{-2} at pH = 14, capacity retention was measured at 91% over 400 cycles at a current density of 0.1 A·cm^{-2}. At 1 M ACA and adjusted cell compression, the capacity retention was measured as 99.95% and EE was 75% at a current density of 0.1 A·cm^{-2} (Fig. 5(e)). The Meng group used FMN with Na$^+$, (FMN-Na, **4b**, Fig. 5(a)), as the negolyte [66]. The poor solubility of FMN-Na, 0.06 M in 1 M KOH, was increased to 1.5 M in the presence of 3 M nicotinamide, while the viscosity rose roughly three-fold (3.2 mPa). The 0.06 M FMA-NA negolyte combined with 0.1 M $K_4[Fe(CN)_6]$ posolyte in 1 M KOH(aq) achieved 1.3 Ah·L^{-1} discharge capacity, ~ 99% capacity retention, and ~ 99% CE over 200 cycles at a current density of 10 mA·cm^{-2}. The increasing concentration of FMN-Na to 0.24 M FMN-Na and the posolyte of 0.4 M $K_4[Fe(CN)_6]$ also achieved similar performance (~ 99% capacity

retention over 100 cycles) at a current density of 80 mA·cm^{-2} and the discharge capacity was increased to ~ 4 Ah·L^{-1}. The authors claimed that the oxidized and the reduced forms of FMN-Na were stabilized from electron delocalization, thus resulting in alleviation of unintended reaction. The reported results are summarized in Table 3.

3.5 TEMPO-based posolyte

For the posolytes, I$^-$/I$_3^-$, Br$^-$/Br$_3^-$, ferrocene derivatives, [Fe(CN)$_6$]$^{4-}$/ [Fe(CN)$_6$]$^{3-}$, and TEMPO have been widely used. Here we focus on the organic radical of TEMPO that is the well-known redox mediator and radical marker. Unlike a typical radical species, TEMPO is highly stable because of the delocalization of electrons between N and O and the steric protection of radicals from four methyl groups. TEMPO shows a reversible and fast 1e$^-$ redox reaction in the potential range of 0.8–1.1 V vs. SHE and forms an oxoammonium salt after the anodic reaction (Fig. 6(a)). Since TEMPO itself is insoluble in water, the hydrophilic group or ionic moiety is decorated at the 4-position of TEMPO, which also shifts the redox potential.

Table 3 A summary of alloxazine derivatives used in aqueous RFBs along with electrochemical properties

Alloxazine derivatives	Posolyte	Solubility in water	Potential/cell potential	Capacity retention	CE, EE	k_0 (cm·s^{-1}) D (cm^2·s^{-1})	Cycles
4a	$K_4Fe(CN)$ + $K_3Fe(CN)_6$	1 M in 1 M KOH	−0.60 V (vs. SHE)/1.2 V	99.98% per cycle	0.1 A·cm^{-2} 99.7%, 74%	1.2×10^{-5} cm·s^{-1}, N/A	400
4b	$K_4Fe(CN)_6$	0.06 M in 1 M KOH and 1.5 M with nicotinamide additive	−0.53 V (vs. SHE)/1.03 V	Average 99%	10 mA·cm^{-2} 99%	5.3×10^{-3} cm·s^{-1}, 1.3×10^{-6} cm^2·s^{-1}	200
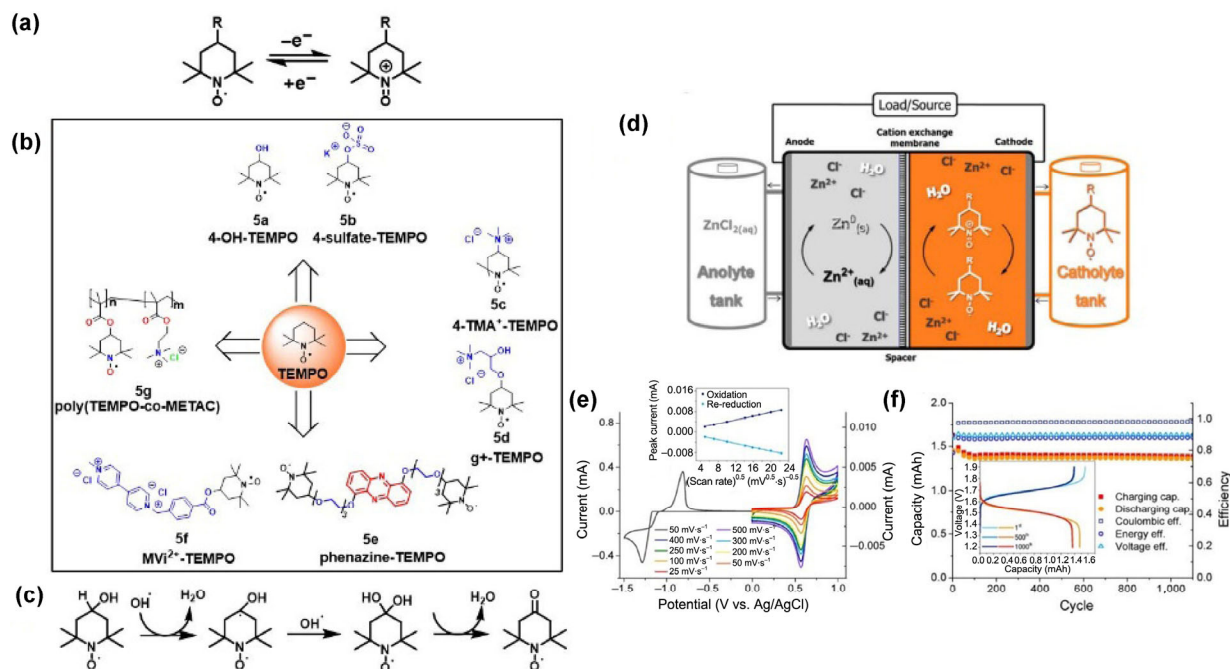
Figure 6 Electrochemical and chemical reactions of TEMPO as the posolyte in aqueous RFBs. (a) Electrochemical reaction process. (b) Various molecular designs of TEMPO. (c) Self-oxidation process of **5a**. (d) Schematic illustration of half-RFB configuration where TEMPO and Zn metal are used as the posolyte and negative electrode, representatively. (e) Cyclic voltammograms of Zn stripping/deposition (black) and redox event of **5b** in ZnCl$_2$/NH$_4$Cl(aq). The sweeping rates for electrochemical reaction of 5b were 25–500 mV·s^{-1}. The inset shows the redox peak as a function of the root of sweeping rate. (f) Cycling performance of aqueous RFB with 0.1 M **5a** || Zn in ZnCl$_2$/NH$_4$Cl(aq) at 40 mA cm^{-2} in a static cell. The inset in (f) shows galvanostatic charge–discharge profiles. (c) is adapted from Ref. [47], © Hoober-Burkhardt, L. et al. 2017. (d)–(f) are reproduced with permission from Ref. [67], © American Chemical Society 2018.

The Wang group introduced the hydroxyl group to the 4-position of TEMPO (4-OH-TEMPO, **5a**, Fig. 6(b)) [59]. The 4-OH-TEMPO has ~ 2.1 M solubility in water while the solubility is decreased to ~ 0.5 M in the presence of 1.5 M NaCl(aq). The diffusion coefficient and the reaction rate of 4-OH-TEMPO were measured as 2.95×10^{-5} and 2.8×10^{-4} cm·s^{-1}, respectively. The RFBs consisting of a posolyte of 0.1 M 4-OH-TEMPO and a negolyte of 0.1 M MVi^{2+} delivered initial capacity of ~ 0.053 Ah at a current density of 40 mA·cm^{-2}, and 99% capacity retention over 100 cycles. At higher current densities of 100 mA·cm^{-2}, the capacity and EE decreased, possibly due to a slow reaction rate. It is well known that self-oxidation *via* hydroxyl radicals make 4-OH-TEMPO unstable, which irreversibly forms (Fig. 6(c)) [44]. Therefore, new designs stabilizing TEMPO were exclusively suggested. The Schubert group exploited the substitution of the sulfonate group at the 4-position, i.e. 4-sulfate-TEMPO (**5b**, Fig. 6(b)), and combined this with aqueous Zn batteries (Fig. 6(d)) [67]. The solubility of 4-sulfate-TEMPO was ~ 1 M in the presence of 2 M ZnCl$_2$ + 2 M NH$_4$Cl. The Zn^0/Zn^{2+} deposition/stripping occurring at the negative electrode of metallic Zn and the redox event of 4-sulfate-TEMPO posolyte have a ~ 1.7 V voltage gap (Fig. 6(e)). This half-RFB showed a capacity retention of 93.6% and 98.1% CE over 1,100 cycles at a current density of 40 mA·cm^{-2} (Fig. 6(f)). By replacing 4-sulfate-TEMPO with 4-OH-TEMPO, fast capacity fading was measured within 300 cycles. The Schubert group added trimethylammonium chloride (TMA$^+$Cl$^-$) salt to the 4-position of TEMPO to yield 4-TMA$^+$-TEMPO (**5c**, Fig. 6(b)) [68]. The cation of TMA$^+$ group increases the solubility to 3.2 M in water and 2.3 M in 1 M NaCl(aq). In addition, the Cl$^-$ can play a role of a charge carrier that transports between the negolyte and posolyte side for charge balance, without requiring extra supporting electrolyte. The RFBs containing 2 M 4-TMA$^+$-TEMPO and 2 M MVi^{2+} showed a cell voltage of 1.4 V and almost full capacity retention over 100 cycles at a current density of 80 mA·cm^{-2}. The Chen group invented a one-pot reaction to produce the cationic TEMPO of g$^+$-TEMPO (**5d**, Fig. 6(b)), by epoxide ring opening of the additional N,N,N-trimethyl-1-(oxiran-2-yl)methanaminium chloride, which has a less tedious synthetic process than the preparation of 4-TMA$^+$-TEMPO [69]. The half-RFB comprised 0.2 M of g$^+$-TEMPO in 1 M NaCl and a Zn metal with 0.3 M ZnCl$_2$/0.3 M NH$_4$Cl(aq), and showed ~ 0.046% capacity fading per cycle at 20 mA·cm^{-2} with a CE of 99.3% over 140 cycles. The same half-RFB but with the inclusion of 4-OH-TEMPO posolyte showed ~ 0.3% capacity fading rate for the initial 30 cycles, demonstrating enhanced stability of TEMPO by the addition of g$^+$.

Despite the above-mentioned functionalization, the crossover of TEMPO derivatives has not been successfully resolved. The Schubert group attempted to develop a combi-molecule where the posolyte of TEMPO was chemically bound with a negolyte molecule, and prepared all combi-molecule RFBs where the combi-molecules play a role of both the negolyte and posolyte, analogous to all VRFBs, which may alleviate the crossover problem. As initial trials, the negolyte role of phenazine and the posolyte role of TEMPO were connected by a triethylene glycol linker (**5e**, Fig. 6(b)) [70]. This 10 mM phenazine-TEMPO was introduced to a symmetric configuration of static cells and a cell voltage of ~ 1.2 V in 0.5 M NaCl(aq) was measured. The cycling test demonstrated negligible capacity fading over 1,800 cycles with a CE of ~ 98.3%, indicating that this combi-molecule successfully acted as both the posolyte and negolyte with less crossover, while the EE was evaluated to be poor at < 50%, due to slow reaction kinetics of the phenazine subunit [71]. In the following study, the Schubert group replaced the phenazine unit with MVi^{2+}, producing a MVi^{2+}-TEMPO (**5f**, Fig. 6(b)) combi-molecule [72]. An additional non-aqueous co-solvent of 20 vol.% ethylene carbonate solution was needed to dissolve the radical cationic form of MVi$^{+\cdot}$ up to 0.1 M in NaCl(aq). In addition, since the substitution of OH to the nitroxide of TEMPO irreversibly produced a hydroxylamine group during the cycling test, the authors tried to add either the acetate or the phosphate buffer to maintain pH of 2–7. However, despite various efforts and tests to find the optimum anion exchange membranes, fast capacity loss was observed within 5–10 cycles.
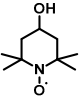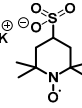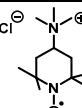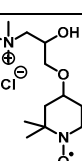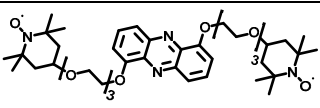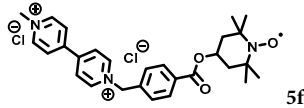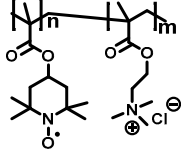
Instead of designing combi-molecules, the polymerization of small TEMPO derivatives is a clear way to prevent crossover. The Schubert group synthesized water soluble, non-conjugated, and low molar mass polymer chains that linked up with TEMPO and MVi^{2+} with a unit level of 0.8–0.9 [73]. The diffusion coefficients of poly(TEMPO) and poly(MVi^{2+}) were measured as 7.0×10^{-8} and 7.6×10^{-7} cm^2·s^{-1}, respectively, which were lower than those of the original small molecules, while the reaction rates were comparable to those of the small molecules, as 4.5×10^{-4} and 9×10^{-5} cm·s^{-1}, for poly(TEMPO) and poly(MVi^{2+}), respectively. The polymer-based posolyte and negolyte were then combined with a cellulose dialysis membrane and NaCl(aq), and these static cells offered 41% of the theoretical capacity and ~ 80% capacity retention over 10,000 cycles at a current density of 20 mA·cm^{-2} [73]. In comparison, the RFBs showed 75% of the theoretical capacity at a current density of 40 mA·cm^{-2}, and a volumetric energy density of ~ 8.0 Wh·L^{-1} during discharge, which is comparable to that of VRFBs. However, the capacity fading rate was considerably high, which the authors ascribed to the oxidation of MVi$^{+\cdot}$ owing to its leakage of a pump tube. The Schubert group also designed TEMPO tethered with various polymer backbones and branches such as [2-(methacryloyloxy)ethyl]trimethylammonium chloride (METAC), i.e. poly(TEMPO-*co*-METAC) (**5g**, Fig. 6(b)), poly(1-methyl-1'-4(-vinylbenzyl)-[4,4'-bipyridine]-1,1'-diium dichloride, and poly(4-methacryloyloxy-2,2,6,6-tetramethylpiperidine-1-oxyl-*co*-2-(methacryloyloxy)-N,N,N-trimethylethane ammonium chloride [74]. The combination of poly(TEMPO-*co*-METAC) with metallic Zn for half-RFBs showed ~ 78.6% capacity retention at 2 mA·cm^{-2} after 1,000 cycles [72].

In short, a stable radical TEMPO has been employed as the posolyte in neutral RFBs. To increase the solubility of TEMPO, diverse hydrophilic and charged substituents have been introduced. The ammonium group-substituted TEMPO showed the most promising result with ~ 3.2 M solubility in water among other alternatives. The crossover of TEMPO is another challenge, and therefore the design of combi-molecule and polymerized-TEMPO has been proposed. The overall results are summarized in Table 4.

4　Future directions for developing aqueous RFBs using nanotechnology

The tuning of the molecular structure and moieties has altered electrochemical and chemical characteristics of redox organic species. Along with such molecular designs as above-mentioned, the design of electrode, redox nanostructural species, and membrane using nanotechnology has been exploited in solving the crucial challenges facing aqueous RFBs. The Kwon group suggested the use of carboxylic acid-functionalized carbon nanotubes (CA-CNTs) mixed with a carbon felt electrode to improve the electrochemical performance of the negolyte of ACA (**4a**) in aqueous RFBs [74]. The deprotonation of the carboxylic acid group in an alkaline solution allows facile interaction between CA-CNTs and nitrogen of –C=N–C– in ACA, which results in increased mass transfer and rate reaction of ACA (Fig. 7(a)). The diffusion coefficient and reaction rate of ACA in the presence of CA-CNTs were measured as 9.4×10^{-4} cm^2·s^{-1} and 3.6×10^{-1} s^{-1}, which were higher than those in the absence of CA-CNTs, i.e., 5.9×10^{-6} cm^2·s^{-1} and 0.2×10^{-2} s^{-1}, respectively. In alkaline RFBs, the CA-CNT/carbon felt electrode alleviated voltage polarization by ~ 30 mV, thus increasing the EE to ~ 64% in comparison

Table 4 A summary of TEMPO derivatives used in aqueous RFBs along with electrochemical properties

TEMPO and derivatives	Negolyte	Solubility in water	Potential/cell potential	Capacity retention	CE, EE
5a	MVi^{2+} (2a)	2.1 M in neutal water and 0.5 M in 1.5 M NaCl	0.8 V (vs. SHE)/1.25 V	99% 100 cycles	40 mA·cm^2 99%, 70.9%
5b	Metallic Zn	1 M in 2 M ZnCl$_2$ + 2 M NH$_4$Cl	0.8 V (vs. SHE)/1.7 V	93.6% 1,100 cycles (3 mA·cm^2)	40 mA·cm^2 98.1%, 65%
5e	MVi^{2+} (2a)	3.2 M in water and 2.3 M in 1 M NaCl	0.95 V (vs SHE)/1.4 V	> 99% 100 cycles	50 mA·cm^2 > 99%, 70%
5d	Metallic Zn	0.2 M in 1 M NaCl	0.8 V (vs. SHE)/1.7 V	99.954% per cycle 140 cycles	20 mA·cm^2 99.3%, 77%
5c	Same as posolyte (combi-molecule)	10 mM in 0.5 M NaCl	0.8 V (vs. SHE)/1.2 V	~ 80% 1,800 cycles	98.3%, < 50%
5f	Same as posolyte (combi-molecule)	25 mM in 0.3 M NaCl + 20 vol.% ethylene carbonate	0.77 V (vs. SHE)/1.16 V	N/A	N/A, N/A
5g	Poly(MVi^{2+})	N/A	0.9 V (vs. SHE)/ 1.1 V	80% 10,000 cycles	20 mA·cm^2 97.5%, 77.5%

with that of carbon felt alone of ~ 60% over 30 cycles (Fig. 7(b)). In addition, the employment of CA-CNTs delivered a discharge capacity of 26.7 Ah·L^{-1}, or ~ 83% of the theoretical capacity, which was larger than 72% in the absence of CA-CNTs (Fig. 7(b)).

As another promising approach, cross-linked polymer-based nanoparticular colloids were employed as the carrier of discrete charge and showed suppression of the crossover issue. The Rodríguez-López group prepared a poly (vinylbenzyl ethylviologen)-based redox active colloid (RAC, Fig. 7(c)) [76]. The redox potential was –0.7 V vs. Ag/Ag$^+$ in the condition of a non-aqueous electrolyte solution (Fig. 7(d)), which was consistent with the potential of a small molecule of Vi^{2+}. Among three different diameters of 80, 135, and 827 nm (Fig. 7(c)), the larger one exhibited the fastest reaction rate and lowest viscosity even at concentrations up to 40 wt.%. In RFBs, all RACs prevented the crossover problem with a > 99% rejection ratio due to their larger size than a porous Celgard membrane, which had a pore size of 28 nm, and this resulted in stable cycling performance over 11 cycles (Fig. 7(e)). Although the ratio of material utilization was only 21%, which was equivalent to ~ 10 mM of Vi^{2+}, some sedimentation was observed from a ferrocene-based RAC as the posolyte in the given non-aqueous electrolyte solution, the first attempt to employ a nanocolloidal redox species shows promise for remarkable mitigation of crossover by the stable RAC maintaining its electrochemical characteristics and spherical shape after cycling.

To suppress the crossover, a fundamental solution is to design a membrane with small-sized pores. A cross-linked PIM-1 polymer approaches < 1.2 nm pore dimension, and shows > 9,000-fold higher blocking ability than a Celgard membrane for oligomer-type redox organic species with 0.88–1.23 nm size in a non-aqueous electrolyte solution [77]. A recently developed sulfonated mesoporous membrane has 3–4 nm pore size in addition to the ability of selective ion permeation in the given pH of an aqueous electrolyte solution [78]. For aqueous VRFBs, the sulfonated mesoporous membrane exhibited 100-fold lower VO^{2+} permeability than a Nafion 117 membrane, and higher discharge capacity retention than Nafion 212.

Taken together, the aforementioned findings demonstrate that the development of critical components in organic RFBs is necessary to ameliorate the electrochemical reactions and avoid unintended reaction processes that lower total cell performance. Nanotechnology is the key to design electrodes, membranes and cages of redox species, which will be evolved in parallel with molecular engineering of redox organic species, for practical applications of organic RFBs in the future.

5   Conclusion and perspectives

In this review, we have summarized recent developments in various redox organic species and their applications in aqueous organic RFBs. Many studies have investigated the well-known redox mediators and biological redox species, and molecular engineering strategies according to the target of the RFB have enhanced their solubility, redox potential shift, and chemical stability. Existing research has demonstrated that redox organic molecules are a promising candidate for redox couples in RFBs.
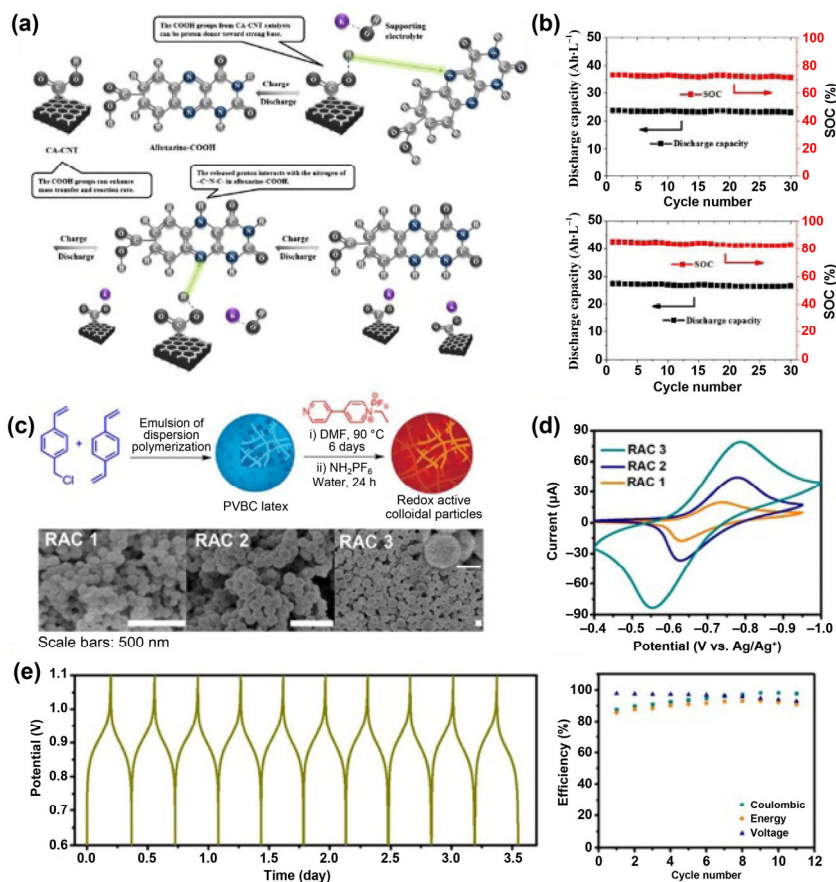
Figure 7 Strategies to improve RFB performance using nanotechnology. (a) Schematic illustration showing the role of carboxylic acid-functionalized CNTs (CA-CNTs) for the negolyte of ACA (**4a**). (b) Comparison of cycling performance profiles for discharging capacity and SOC for ACA-based RFB (top) without CA-CNTs, (bottom) with CA-CNT catalyst. (c) Preparation of redox-active colloids (RACs, top) and scanning electron microscopy (SEM) images of Vi^{2+}-based RACS with three different sizes, 80, 135, and 827 nm for RAC 1, 2, and 3, respectively (bottom). (d) Cyclic voltammograms of Vi^{2+}-RACs with different sizes at a sweeping rate of 20 mV·s^{-1} in 0.1 M LiBF$_4$ in acetonitrile. (e) Galvanostatic cycling performance (left) and the corresponding CE (right) of a RFB with 10 mM RAC 2 ∥ ferrocene-based RAC in 0.1 M LiBF$_4$/acetonitrile at 43 μA·cm^{-2} over 11 cycles. (a) and (b) are reproduced with permission from Ref. [75], © American Chemical Society 2018. (c)–(e) are reproduced with permission from Ref. [76], © American Chemical Society 2016.

However, a great deal of work should still be done to evolve advanced organic species. Most studies have used small concentrations of redox organic species due to the limitation of solubility and undesired chemical reactions. To develop practical redox couples and evaluate true performance of RFBs, increasing concentration of redox species in line with the stringent criteria for RFB applications should be necessary. The solubility for cathodic/anodic forms is also examined to ensure the capability of redox species for reversible electrochemical reactions. In addition, undesired reactions between redox species and between redox species and electrolyte solution are carefully diagnosed at variant states of discharge and charge through *in situ* and *ex situ* analytical methods, which allows us to understand chemical-reaction pathways. The functionalization of redox molecules pursued to improve chemical stability, while the initiative studies to dig out new redox species would also be attempted. Computational studies can open up new perspectives in molecular design and facilitate the prediction of electrochemical properties and reaction pathways, which can notably reduce labor-intensive, time-consuming and error-prone tasks [33–35]. In terms of molecular synthesis, advanced synthetic methods should be explored to yield mass production through easy, short, and economical synthetic routes. Development of comprehensive cost-models will be helpful in estimating operational costs and reducing the total synthetic expense. Lastly, the high-cost and crossover issue of membranes are the central challenges for all RFBs including current technology of vanadium RFBs. The economical membranes that are optimized for aqueous RFB can spur the growth of RFB technology. The

nanotechnology can contribute to innovative design of membranes by modifying their pore-size and decorating ionic landscape, thus increasing power density and cycling performance. All these efforts could enable organic RFBs to become more appealing for their widespread use in grid-scale energy storage systems.

Acknowledgements

References

[1] Dresselhaus, M. S.; Thomas, I. L. Alternative energy technologies. *Nature* **2001**, *414*, 332–337.

[2] Sternberg, A.; Bardow, A. Power-to-what?—Environmental assessment of energy storage systems. *Energy Environ. Sci.* **2015**, *8*, 389–400.

[3] Yang, Z. G.; Zhang, J. L.; Kintner-Meyer, M. C. W.; Lu, X. H.; Choi, D.; Lemmon, J. P.; Liu, J. Electrochemical energy storage for green grid. *Chem. Rev.* **2011**, *111*, 3577–3613.

[4] Larcher, D.; Tarascon, J. M. Towards greener and more sustainable batteries for electrical energy storage. *Nat. Chem.* **2015**, *7*, 19–29.

[5] Dunn, B.; Kamath, H.; Tarascon, J. M. Electrical energy storage for the grid: A battery of choices. *Science* **2011**, *334*, 928–935.

[6] Zakeri, B.; Syri, S. Electrical energy storage systems: A comparative life cycle cost analysis. *Renew. Sustain. Energy Rev.* **2015**, *42*, 569–596.

[7] Tarascon, J. M.; Armand, M. Issues and challenges facing rechargeable lithium batteries. In *Materials for Sustainable Energy*; Dusastre, V., Ed.;

Co-Published with Macmillan Publishers Ltd: UK, 2010; pp 171–179.

[8] Hu, L. B.; Zhang, S. S.; Zhang, Z. C. Electrolytes for lithium and lithium-ion batteries. In *Rechargeable Batteries*; Zhang, Z. C.; Zhang, S. S., Eds.; Springer: Cham, 2015; pp 231–261.

[9] Ding, Y.; Zhang, C. K.; Zhang, L. Y.; Zhou, Y. G.; Yu, G. H. Molecular engineering of organic electroactive materials for redox flow batteries. *Chem. Soc. Rev.* **2018**, *47*, 69–103.

[10] Alotto, P.; Guarnieri, M.; Moro, F. Redox flow batteries for the storage of renewable energy: A review. *Renew. Sustain. Energy Rev.* **2014**, *29*, 325–335.

[11] Chen, H. N.; Cong, G. T.; Lu, Y. C. Recent progress in organic redox flow batteries: Active materials, electrolytes and membranes. *J. Energy Chem.* **2018**, *27*, 1304–1325.

[12] Duan, W.; Kizewski, J. P.; Wang, W. Introduction to redox flow batteries. In *Redox Flow Batteries*; CRC Press: 2017; pp 43–76.

[13] Liu, W. Q.; Lu, W. J.; Zhang, H. M.; Li, X. F. Aqueous flow batteries: Research and development. *Chem.—Eur. J.* **2019**, *25*, 1649–1664.

[14] Weber, A. Z.; Mench, M. M.; Meyers, J. P.; Ross, P. N.; Gostick, J. T.; Liu, Q. H. Redox flow batteries: A review. *J. Appl. Electrochem.* **2011**, *41*, 1137–1164.

[15] Kim, K. J.; Park, M. S.; Kim, Y. J.; Kim, J. H.; Dou, S. X.; Skyllas-Kazacos, M. A Technology review of electrodes and reaction mechanisms in vanadium redox flow batteries. *J. Mater. Chem. A* **2015**, *3*, 16913–16933.

[16] Ulaganathan, M.; Aravindan, V.; Yan, Q. Y.; Madhavi, S.; Skyllas−Kazacos, M.; Lim, T. M. Recent advancements in all−vanadium redox flow batteries. *Adv. Mater. Interfaces* **2016**, *3*, 1500309.

[17] Choi, C.; Kim, S.; Kim, R.; Choi, Y.; Kim, S.; Jung, H. Y.; Yang, J. H.; Kim, H. T. A review of vanadium electrolytes for vanadium redox flow batteries. *Renew. Sustain. Energy Rev.* **2017**, *69*, 263–274.

[18] Xu, Q.; Ji, Y. N.; Qin, L. Y.; Leung, P. K.; Qiao, F.; Li, Y. S.; Su, H. N. Evaluation of redox flow batteries goes beyond round-trip efficiency: A technical review. *J. Energy Storage* **2018**, *16*, 108–115.

[19] Yoon, A. K. Y.; Noh, H. S.; Yoon, Y. S. Analysis of vanadium redox flow battery cell with superconducting charging system for solar energy. *Elect. Electron. Eng.* **2016**, *6*, 1–5.

[20] Butler, P. C.; Eidler, P. A.; Grimes, P. G.; Klassen, S. E.; Miles, R. C. Zinc/bromine batteries. *Handbook of Batteries*; Linden, D.; Reddy, T. B., Eds.; McGraw-Hill: Ohio, 2001; pp 37–01.

[21] Lai, Q. Z.; Zhang, H. M.; Li, X. F.; Zhang, L. Q.; Cheng, Y. H. A novel single flow zinc–bromine battery with improved energy density. *J. Power Sources*, **2013**, *235*, 1–4.

[22] Zhao, Y; Wang, L. N.; Byon, H. R. High-performance rechargeable lithium-iodine batteries using triiodide/iodide redox couples in an aqueous cathode. *Nat. Commun.*, **2013**, *4*, 1896.

[23] Weng, G. M.; Li, Z. J.; Cong, G. T.; Zhou, Y. C.; Lu, Y. C. Unlocking the capacity of iodide for high-energy-density zinc/polyiodide and lithium/polyiodide redox flow batteries. *Energy Environ. Sci.* **2017**, *10*, 735–741.

[24] Hu, B.; DeBruler, C.; Rhodes, Z.; Liu, T. L. Long-cycling aqueous organic redox flow battery (AORFB) toward sustainable and safe energy storage. *J. Am. Chem. Soc.* **2017**, *139*, 1207–1214.

[25] Wang, W.; Sprenkle, V. Redox flow batteries go organic. *Nat. Chem.* **2016**, *8*, 204–206.

[26] Winsberg, J.; Hagemann, T.; Janoschka, T.; Hager, M. D.; Schubert, U. S. Redox-flow batteries: From metals to organic redox-active materials. *Angew. Chem., Int. Ed.* **2017**, *56*, 686–711.

[27] Kowalski, J. A.; Su, L.; Milstein, J. D.; Brushett, F. R. Recent advances in molecular engineering of redox active organic molecules for nonaqueous flow batteries. *Curr. Opin. Chem. Eng.* **2016**, *13*, 45–52.

[28] Wei, X. L.; Pan, W. X.; Duan, W. T.; Hollas, A.; Yang, Z.; Li, B.; Nie, Z. M.; Liu, J.; Reed, D.; Wang, W. et al. Materials and systems for organic redox flow batteries: Status and challenges. *ACS Energy Lett.* **2017**, *2*, 2187–2204.

[29] Park, M.; Ryu, J.; Wang, W.; Cho, J. Material design and engineering of next-generation flow-battery technologies. *Nat. Rev. Mater.* **2016**, *2*, 16080.

[30] Armstrong, C. G.; Toghill, K. E. Stability of molecular radicals in organic non-aqueous redox flow batteries: A mini review. *Electrochem. Commun.* **2018**, *91*, 19–24.

[31] Pakiari, A. H.; Siahrostami, S.; Mohajeri, A. Application of density functional theory for evaluation of standard two-electron reduction potentials in some quinone derivatives. *J. Mol. Struct. THEOCHEM* **2008**, *870*, 10–14.

[32] Pelzer, K. M.; Cheng, L.; Curtiss, L. A. Effects of functional groups in redox-active organic molecules: A high-throughput screening approach. *J. Phys. Chem. C* **2017**, *121*, 237–245.

[33] Ding, Y.; Li, Y. F.; Yu, G. H. Exploring bio-inspired quinone-based organic redox flow batteries: A combined experimental and computational study. *Chem* **2016**, *1*, 790–801.

[34] Bachman, J. E.; Curtiss, L. A.; Assary, R. S. Investigation of the redox chemistry of anthraquinone derivatives using density functional theory. *J. Phys. Chem. A* **2014**, *118*, 8852–8860.

[35] Er, S.; Suh, C.; Marshak, M. P.; Aspuru-Guzik, A. Computational design of molecules for an all-quinone redox flow battery. *Chem. Sci.* **2015**, *6*, 885–893.

[36] Yang, C. Z.; Nikiforidis, G.; Park, J. Y.; Choi, J.; Luo, Y.; Zhang, L.; Wang, S. C.; Chan, Y. T.; Lim, J.; Hou, Z. M. et al. Designing redox-stable cobalt–polypyridyl complexes for redox flow batteries: Spin-crossover delocalizes excess charge. *Adv. Energy Mater.* **2018**, *8*, 1702897.

[37] Yang, Z. J.; Tong, L. C.; Tabor, D. P.; Beh, E. S.; Goulet, M. A.; De Porcellinis, D.; Aspuru-Guzik, A.; Gordon, R. G.; Aziz, M. J. Alkaline benzoquinone aqueous flow battery for large-scale storage of electrical energy. *Adv. Energy Mater.* **2018**, *8*, 1702056.

[38] Quan, M.; Sanchez, D.; Wasylkiw, M. F.; Smith, D. K. Voltammetry of quinones in unbuffered aqueous solution: Reassessing the roles of proton transfer and hydrogen bonding in the aqueous electrochemistry of quinones. *J. Am. Chem. Soc.* **2007**, *129*, 12847–12856.

[39] Bird, C. L.; Kuhn, A. T. Electrochemistry of the viologens. *Chem. Soc. Rev.* **1981**, *10*, 49–82.

[40] Hu, B.; Tang, Y. J.; Luo, J.; Grove, G.; Guo, Y. S.; Liu, T. L. Improved radical stability of viologen anolytes in aqueous organic redox flow batteries. *Chem. Commun.* **2018**, *54*, 6871–6874.

[41] Luo, J.; Hu, B.; Debruler, C.; Liu, T. L. A π-conjugation extended viologen as a two-electron storage anolyte for total organic aqueous redox flow batteries. *Angew. Chem., Int. Ed.* **2018**, *57*, 231–235.

[42] DeBruler, C.; Hu, B.; Moss, J.; Liu, X.; Luo, J.; Sun, Y. J.; Liu, T. L. Designer two-electron storage viologen anolyte materials for neutral aqueous organic redox flow batteries. *Chem* **2017**, *3*, 961–978.

[43] Penzkofer, A.; Tyagi, A.; Kiermaier, J. Room temperature hydrolysis of lumiflavin in alkaline aqueous solution. *J. Photochem. Photobiol. A Chem.* **2011**, *217*, 369–375.

[44] Marshall, D. L.; Christian, M. L.; Gryn'ova, G.; Coote, M. L.; Barker, P. J.; Blanksby, S. J. Oxidation of 4-substituted TEMPO derivatives reveals modifications at the 1- and 4-positions. *Org. Biomol. Chem.* **2011**, *9*, 4936–4947.

[45] Kurreck, H.; Huber, M. Model reactions for photosynthesis—Photoinduced charge and energy transfer between covalently linked porphyrin and quinone units. *Angew. Chem., Int. Ed.* **1995**, *34*, 849–866.

[46] Scott, D. T.; McKnight, D. M.; Blunt-Harris, E. L.; Kolesar, S. E.; Lovley, D. R. Quinone moieties act as electron acceptors in the reduction of humic substances by humics-reducing microorganisms. *Environ. Sci. Technol.* **1998**, *32*, 2984–2989.

[47] Hoober-Burkhardt, L.; Krishnamoorthy, S.; Yang, B.; Murali, A.; Nirmal-chandar, A.; Prakash, G. K. S.; Narayanan, S. R. A new michael-reaction-resistant benzoquinone for aqueous organic redox flow batteries. *J. Electrochem. Soc.* **2017**, *164*, A600–A607.

[48] Ding, Y.; Yu, G. H. A bio-inspired, heavy-metal-free, dual-electrolyte liquid battery towards sustainable energy storage. *Angew. Chem., Int. Ed.* **2016**, *55*, 4772–4776.

[49] Xu, Y.; Wen, Y. H.; Cheng, J.; Yanga, Y. S.; Xie, Z. L.; Cao, G. P. Novel organic redox flow batteries using soluble quinonoid compounds as positive materials. In *Proceedings of 2009 World Non-Grid-Connected Wind Power and Energy Conference*, Nanjing, China, 2009.

[50] Yang, B.; Hoober-Burkhardt, L.; Wang, F.; Surya Prakash, G. K.; Narayanan, S. R. An inexpensive aqueous flow battery for large-scale electrical energy storage based on water-soluble organic redox couples. *J. Electrochem. Soc.* **2014**, *161*, A1371–A1380.

[51] Wedege, K.; Dražević, E.; Konya, D.; Bentien, A. Organic redox species in aqueous flow batteries: Redox potentials, chemical stability and solubility. *Sci. Rep.* **2016**, *6*, 39101.

[52] Wang, C. X.; Yang, Z.; Wang, Y. R.; Zhao, P. Y.; Yan, W.; Zhu, G. Y.; Ma, L. B.; Yu, B.; Wang, L.; Li, G. G. et al. High-performance alkaline organic redox flow batteries based on 2-hydroxy-3-carboxy-1,4-naphthoquinone. *ACS Energy Lett.* **2018**, *3*, 2404–2409.

[53] Gerhardt, M. R.; Tong, L. C.; Gómez-Bombarelli, R.; Chen, Q.; Marshak, M. P.; Galvin, C. J.; Aspuru-Guzik, A.; Gordon, R. G.; Aziz, M. J. Anthraquinone derivatives in aqueous flow batteries. *Adv. Energy Mater.* **2017**, *7*, 1601488.

[54] Huskinson, B.; Marshak, M. P.; Suh, C.; Er, S.; Gerhardt, M. R.; Galvin, C. J.; Chen, X. D.; Aspuru-Guzik, A.; Gordon, R. G.; Aziz, M. J. A metal-free organic-inorganic aqueous flow battery. *Nature* **2014**, *505*, 195–198.

[55] Carretero-González, J.; Castillo-Martínez, E.; Armand, M. Highly water-soluble three-redox state organic dyes as bifunctional analytes. *Energy Environ. Sci.* **2016**, *9*, 3521–3530.

[56] Lin, K. X.; Chen, Q.; Gerhardt, M. R.; Tong, L. C.; Kim, S. B.; Eisenach, L.; Valle, A. W.; Hardee, D.; Gordon, R. G.; Aziz, M. J. et al. Alkaline quinone flow battery. *Science* **2015**, *349*, 1529–1532.

[57] Kwabi, D. G.; Lin, K. X.; Ji, Y. L.; Kerr, E. F.; Goulet, M. A.; De Porcellinis, D.; Tabor, D. P.; Pollack, D. A.; Aspuru-Guzik, A.; Gordon, R. G. et al. Alkaline quinone flow battery with long lifetime at pH 12. *Joule* **2018**, *2*, 1894–1906.

[58] Michaelis, L.; Hill, E. S. The viologen indicators. *J. Gen. Physiol.* **1933**, *16*, 859–873.

[59] Liu, T. B.; Wei, X. L.; Nie, Z. M.; Sprenkle, V.; Wang, W. A total organic aqueous redox flow battery employing a low cost and sustainable methyl viologen anolyte and 4-HO-TEMPO catholyte. *Adv. Energy Mater.* **2016**, *6*, 1501449.

[60] Beh, E. S.; De Porcellinis, D.; Gracia, R. L.; Xia, K. T.; Gordon, R. G.; Aziz, M. J. A neutral pH aqueous organic–organometallic redox flow battery with extremely high capacity retention. *ACS Energy Lett.* **2017**, *2*, 639–644.

[61] DeBruler, C.; Hu, B.; Moss, J.; Luo, J.; Liu, T. L. A sulfonate-functionalized viologen enabling neutral cation exchange, aqueous organic redox flow batteries toward renewable energy storage. *ACS Energy Lett.* **2018**, *3*, 663–668.

[62] Skyllas-Kazacos, M.; Chakrabarti, M. H.; Hajimolana, S. A.; Mjalli, F. S.; Saleem, M. Progress in flow battery research and development. *J. Electrochem. Soc.* **2011**, *158*, R55–R79.

[63] Miura, R. Versatility and specificity in flavoenzymes: Control mechanisms of flavin reactivity. *Chem. Rec.* **2001**, *1*, 183–194.

[64] Hong, J.; Lee, M.; Lee, B.; Seo, D. H.; Park, C. B.; Kang, K. Biologically inspired pteridine redox centres for rechargeable batteries. *Nat. Commun.* **2014**, *5*, 5335.

[65] Lin, K. X.; Gómez-Bombarelli, R.; Beh, E. S.; Tong, L. C.; Chen, Q.; Valle, A.; Aspuru-Guzik, A.; Aziz, M. J.; Gordon, R. G. A redox-flow battery with an alloxazine-based organic electrolyte. *Nat. Energy* **2016**, *1*, 16102.

[66] Orita, A.; Verde, M. G.; Sakai, M.; Meng, Y. S. A biomimetic redox flow battery based on flavin mononucleotide. *Nat. Commun.* **2016**, *7*, 13230.

[67] Winsberg, J.; Stolze, C.; Schwenke, A.; Muench, S.; Hager, M. D.; Schubert, U. S. Aqueous 2,2,6,6-tetramethylpiperidine-*N*-oxyl catholytes for a high-capacity and high current density oxygen-insensitive hybrid-flow battery. *ACS Energy Lett.* **2017**, *2*, 411–416.

[68] Janoschka, T.; Martin, N.; Hager, M. D.; Schubert, U. S. An aqueous redox-flow battery with high capacity and power: The TEMPTMA/MV system. *Angew. Chem., Int. Ed.* **2016**, *55*, 14427–14430.

[69] Chang, Z. J.; Henkensmeier, D.; Chen, R. Y. One-step cationic grafting of 4-hydroxy-TEMPO and its application in a hybrid redox flow battery with a crosslinked PBI membrane. *ChemSusChem* **2017**, *10*, 3193–3197.

[70] Winsberg, J.; Stolze, C.; Muench, S.; Liedl, F.; Hager, M. D.; Schubert, U. S. TEMPO/phenazine combi-molecule: A redox-active material for symmetric aqueous redox-flow batteries. *ACS Energy Lett.* **2016**, *1*, 976–980.

[71] Hollas, A.; Wei, X. L.; Murugesan, V.; Nie, Z. M.; Li, B.; Reed, D.; Liu, J.; Sprenkle, V.; Wang, W. A biomimetic high-capacity phenazine-based anolyte for aqueous organic redox flow batteries. *Nat. Energy* **2018**, *3*, 508–514.

[72] Janoschka, T.; Friebe, C.; Hager, M. D.; Martin, N.; Schubert, U. S. An approach toward replacing vanadium: A single organic molecule for the anode and cathode of an aqueous redox-flow battery. *ChemistryOpen* **2017**, *6*, 216–220.

[73] Janoschka, T.; Martin, N.; Martin, U.; Friebe, C.; Morgenstern, S.; Hiller, H.; Hager, M. D.; Schubert, U. S. An aqueous, polymer-based redox-flow battery using non-corrosive, safe, and low-cost materials. *Nature* **2015**, *527*, 78–81.

[74] Winsberg, J.; Janoschka, T.; Morgenstern, S.; Hagemann, T.; Muench, S.; Hauffman, G.; Gohy, J. F.; Hager, M. D.; Schubert, U. S. Poly(TEMPO)/zinc hybrid-flow battery: A novel, "green", high voltage, and safe energy storage system. *Adv. Mater.* **2016**, *28*, 2238–2243.

[75] Lee, W.; Kwon, B. W.; Kwon, Y. Effect of carboxylic acid-doped carbon nanotube catalyst on the performance of aqueous organic redox flow battery using the modified alloxazine and ferrocyanide redox couple. *ACS Appl. Mater. Interfaces* **2018**, *10*, 36882–36891.

[76] Montoto, E. C.; Nagarjuna, G.; Hui, J. S.; Burgess, M.; Sekerak, N. M.; Hernández-Burgos, K.; Wei, T. S.; Kneer, M.; Grolman, J.; Cheng, K. J. et al. Redox active colloids as discrete energy storage carriers. *J. Am. Chem. Soc.* **2016**, *138*, 13230–13237.

[77] Doris, S. E.; Ward, A. L.; Baskin, A.; Frischmann, P. D.; Gavvalapalli, N.; Chénard, E.; Sevov, C. S.; Prendergast, D.; Moore, J. S.; Helms, B. A. Macromolecular design strategies for preventing active-material crossover in non-aqueous all-organic redox-flow batteries. *Angew. Chem., Int. Ed.* **2017**, *56*, 1595–1599.

[78] Jeon, C.; Han, J. J.; Seo, M. Control of ion transport in sulfonated mesoporous polymer membranes. *ACS Appl. Mater. Interfaces* **2018**, *10*, 40854–40862.